Funded by the European Union

Compact

XLS-Report-2019-005
27 June 2019

XLS Deliverable D6.1

Computer codes for the facility design

Avni Aksoy[1)*], Anna Giribono[†], Andrea Latina[‡], Héctor Mauricio Castañeda Cortés[§], Neil Thompson[§], Federico Nguyen[†], Edu Marin[¶]

On behalf of the CompactLight Partnership

Prepared on: 27.06.2019

[*] Ankara University, Turkey, [†] ENEA, Italy, [‡] CERN, Switzerland, [§] STFC, United Kingdom, [¶] ALBA-CELLS, Spain

[1] Corresponding author: avni.aksoy@cern.ch

This project is funded by the European Union's Horizon2020 research and innovation programme under Grant Agreement No. 777431. The contents of this report reflect only the view of the CompactLight Consortium. The European Commission is not responsible for any use that may be made of the information it contains.

Abstract

In this deliverable we report an overview of the available tools to perform start to end simulations for the CompacLight facility, covering the beam transport from the cathode to the undulator exit, including space charge effects, coherent synchrotron radiation in magnetic compressors, wakefield effects in the X-band linac and FEL performance. The main objective of WP6 is to provide the key parameters and performance estimates of a facility which meets the user requirements. We need to develop consistent tools for modelling the machine, as the basis for the final integrated performance studies. To this end the tasks of WP6 can be split into three simulation sections, in parallel to facility sections

- Low energy injector (including gun, prelinac and first bunch compressor)
- High energy linac (including high energy BCs for both soft and hard X-Ray layout)
- FEL production (both soft and hard X-Ray FELs)

Different simulation tools have been used by the collaborating institutions suitable for the problems mentioned above. All programs used by the team will be utilized during the course of CompactLight design in order to benefit the experience of partners. However, to perform an integrated simulation one of the existing tool for each section is going to be used. Many of the those tools have been evaluated properly on specific problem for each tool and capabilities has been summarized in this report. In addition, the requirement for the translator tool between each code has been discussed.

Contents

1 Introduction

The main objective of the CompactLight project is to perform a design study which aims to globally optimise the performances and costs of the different parts of the facility: injector, linac and photon production. Clearly each of these sections have many intersections thus start to end optimisation will comprise a large number of parameters.

Different injector schemes are being investigated including RF gun at different operating frequencies (S, C and X band) and following pre-linac accelerator at different operating frequencies (S, C and X band). Normal conducting X-band technology which can provide efficient, high-gradient acceleration with the possibility of high repetition rate operation has been chosen for the main accelerating section. In parallel to X-band technology, new undulator technology employed in the FEL generation section (for example, superconducting undulator technology) will reduce the dimension of the facility.

Reducing the required electron beam energy through the use of more advanced undulators results in savings in civil construction as well as the operation cost of an X-Ray FEL facility. The aim of developing a common facility design, with lower beam energy and more compact. will result in a much lower construction cost and a much lower running cost making X-ray FELs more affordable.

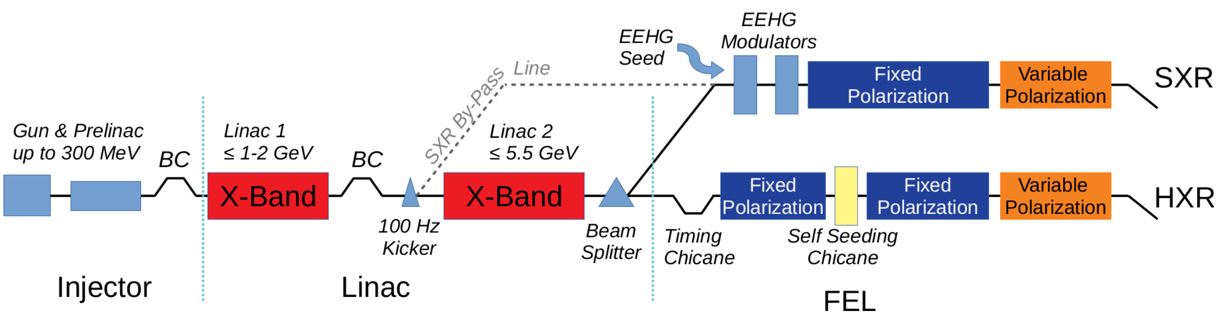

Figure 1: The preliminary layout of the proposed facility

Based on the inputs from the user community a comprehensive photon output specification, summarised in Table 1 has been determined [1]. A preliminary layout of the CompactLight facility which aims to cover the requirements of the user community is shown in Figure 1. A key request from the user community, which affects the facility layout significantly, is large wavelength separation when operating in two colour mode. This effectively means that two bunches must independently reach saturation in two different undulators. To this end, instead of using a long undulator section tuned for two different wavelengths we have proposed to operate two parallel undulator sections, which has several additional advantages. First, the total undulator length is approximately the same and so the parallel option is more compact overall; second, the two independent wavelengths could be combined into a single experiment or, if that is not required, two experiments could take place at the same time, doubling the capacity of the facility.

The 1000 Hz repetition rate given in Table 1 is a very challenging target for many systems, and we might have to compromise on this ambition during the course of the Design Study. On the other hand 100 Hz option is somewhat more relaxed which allows operation of both FEL lines in parallel. When running in hard X-ray at 100 Hz repetition we propose to accelerate two bunch per pulse. One of the bunches in the train will be kicked via a by-pass line to the SXR line while the other will be accelerated up to 5.5 GeV for HXR. In order to run the facility at

Table 1: Main parameters of the CompactLight FEL.

Parameter	Unit	Soft X-ray	Hard X-ray
Photon Energy	keV	0.25-2.0	2.0-16.0
Photon Wavelength	nm	5.0-0.6	0.6-0.08
Repetition rate	Hz	1000	100
Pulse duration	fs	0.1-50	1-50
Polarization		Variable, selectable	
Two-pulse delay	fs	$\pm$ 100	$\pm$ 100
Two-colour separation	%	20	10
Synchronization	fs	< 10	< 10

1000 Hz repetition rate the gradient of linac will be reduced significantly which means the entire facility will reach an energy only sufficient for SXR. A repetition rate of 1000 Hz for the soft-X-ray FEL will be a unique and highly desirable feature of our facility. We are also considering additional concepts, which include seeding in both FELs and a bypass line at 2-$\tilde{2}$.5 GeV so that one FEL could run soft X-ray and the other hard X-ray, both at 100 Hz.

Particle tracking runs of photo-injectors and the following accelerating structures have been done assuming a 65 MV/m accelerating gradient in the main X-Band based linac at 100 Hz repetition rate. Injector optimisation studies have addressed the minimisation of the transverse projected and sliced emittances. Two sage magnetic bunch compressors (BC1 + BC2) are employed to reach a peak current of 5 kA at the end of linac. Table 2 lists the main electron beam parmaters at the FEL for the 100 Hz repetition rate scenario.

Table 2: Main electron beam parameters of the CompactLight FEL.

Parameter	Unit	Soft X-ray	Hard X-ray
Beam Energy	GeV	2.5	5.5
Bunch Charge	pC	<100	<100
Normalized Emittance	mm-mrad	<0.4	<0.4
Max Peak Current	kA	5	5
Min Bunch Length	fs	2	2
RMS slice energy spread	%	0.01	0.01

In this deliverable we report an overview of the available tools to perform start to end simulations for CompactLight, covering the beam transport from the cathode to the undulator exit, including space charge effects, coherent synchrotron radiation in magnetic compressors, wakefield effects in the X-band linac and FEL performance. The main objective of WP6 is to provide the key parameters and performance estimates of a facility which meets the user requirements. We need to develop consistent tools for modelling the machine, as the basis for the final integrated performance studies. To this end the tasks of WP6 can be split into three simulation sections, in parallel to the facility sections

- Low energy injector (including gun, prelinac and first bunch compressor)
- High energy linac (including high energy BCs for both soft and hard X-Ray layout)
- FEL production (both soft and hard X-Ray FELs)

Different simulation tools have been used by the collaborating institutions suitable for the problems mentioned above. However, to perform an integrated simulation one of the existing tools for each section has to be chosen (or we must develop new one(s) if available ones are not convenient.)

In order to compare the available simulation tools we have considered one option for each section. In addition to investigating the sections independently, the sections have been have been somehow simplified in order to give a better comparison of the simulation tools. The CompactLight sections taken into account and corresponding tools to be evaluated are summarised as following;

- S-Band based Low energy injector up to 300 MeV using `ASTRA`, `GPT` , `TStep`, and `RF-Track`;
- X-Band based High energy Linac up to 6 GeV using `ELEGANT` and `PLACET`;
- Hard X-Ray FEL beamline; for 0.77 Å wavelength (16 keV photon energy) using `PERSEO`, `GENESIS`, and two semi-analytic models.

Since all simulation tools are well established for various problems in literature, and have advantages compared to others for some specific problem, most of them are going to be used during the course of the CompactLight design. In the following sections we provide brief information about the simulation tools and compare them on specific problems.

2 Summary of the simulation tools

Start-to-end (S2E) modelling of free-electron lasers (FELs) normally requires the use of multiple codes to correctly capture the physics in each region of the machine. Codes such as `ASTRA`[2], `GPT`[3], `TStep`[4] or `RF-Track`[5], for instance, may be used to simulate the injectors where space charge effects are dominant. From injector the linac and transport line may be handled by codes such as `ELEGANT`[6] or `PLACET`[7]. The necessity for very high peak current requires sensitive tuning for dispersive sections along the beamline. This case may also be simulated by `LiTrack`[8] or `Track1D`[9] in order to make a fast optimization of the bunch compressors. Finally, at the FEL a 1D code `PERSEO`[10] as well as a 3D time dependent code `GENESIS`[11, 12] must be used in addition to analytical formalism. These codes may be optimised to work with a wide range of macro-particle numbers and have different input/output formats. Therefore it is necessary to have translators to provide a bridge between each section for various simulation codes. It is essential that these translators can preserve the statistical properties of the bunch while raising or lowering the number of macro-particles used between codes.

In this section we summarise the simulation tools to be used for CompactLight optimisation. As mentioned earlier, due to the physical problems to be evaluated in different sections of the machine, it is not possible to use a single code from cathode to the end of the x-ray line. A brief description of the FEL codes which are currently used by the members of the CompactLight collaboration (`PERSEO` and `GENESIS`), together with the semi-analytical methods which are used for the optimisation of the FEL performance, is found in the sub-subsection (3.3.1) of this document.

The beam intensity and the beam brightness in an accelerator for driving a FEL are often severely limited by "collective effects". The term "collective effects" refers to the interaction of beam particles with each other through a variety of processes. One can mention many collective effects in an accelerator [13] but tackling the following would be sufficient for CompactLight:

- existence of self-fields and image fields even for constant perfectly conducting and magnetic boundaries (direct and indirect "space-charge effects") at low energies
- electromagnetic "wakefields" of the beam due to a finite chamber resistivity or geometric variation in the beam-pipe/path cross section, which typically affect the back of the bunch
- coherent synchrotron radiation (CSR) which occurs on a curved trajectory of an ultra-relativistic beam which may even influence earlier parts of the beam bunch, giving rise to "non-causal" wakefields.

S2E simulation requires modelling beam properties through all stages of a machine by taking into account all the effects mentioned above. In the absence of such a simulation, FEL modelling is typically performed by using the ideal beam properties from a linac. In addition to the collective effects one shall include machine imperfections, both longitudinal and transversely, to define the key tolerances and mitigation strategies.

2.1 Low Energy Section

Space charge force restrains the brightness of electron RF guns and photo-injectors. For these injectors an efficient compensation scheme based on solenoid focusing was first proposed by Carlsten [14]. However the requirement for very small rms sliced emittance plays a key role in limiting bunch charge and bunch length at the gun stage as well as the requirement for the gradient in the gun. The space charge force is weak and often neglected when the beam energy reaches 100 MeVs for bunch charges of $\approx$ 100 pC [15].

Space charge effects can be calculated using codes which usually run in two steps. The first step is to update the macro particle coordinates as a result of the space charge effects integrated in each small time step. The second step is to transport the macro particle coordinates in the same time period, which is entirely determined by the external lattice elements. Separation of the two parts, and alternative evaluation of them, depends on local details of the beam envelope and the s-dependent space charge potential, where s is the direction of the beam travel. If the transverse and longitudinal beam size evolves, the space charge potential is updated so that the calculation is self-consistent. Calculation for space charge effects can be complex and require high CPU power, depending on the model for space charge potential. Space charge codes solve the interaction between the beam and the self-induced and external fields through integral methods where the fields are derived at each time step from the particle coordinates and momenta in the quasi-static approximation, i.e. solving the Poisson equations in the particles' moving frame. The beam is then modelled as an ensemble of macro-particles, each with an equivalent charge, to which the codes apply the momentum kicks coming from collective effects. The second part, the macro-particle interaction with external fields, is free from space charge and can be straightforward.

Various established space charge codes are used by the partners of CompactLight. In particular the beam dynamics in the low energy section of CompactLight is simulated with three well established tools for the study of charged particle dynamics in electromagnetic fields i.e. the multi-particles codes `TStep`, an heir of `PARMELA` [4], `ASTRA`[2] and `GPT`[3]. We also tested a new code that was developed at CERN during the last few years, `RF-Track`[5]. The codes are briefly described below:

2.1.1 TStep

`TStep` is a widespread reliable multi-particle code that transforms the beam, represented by a collection of particles, through a user-specified linac and/or transport system, where field maps of magnets and accelerator cavities are derived from codes such as `POISSON`, `SUPERFISH` and `HFSS` [16, 17]. It calculates the self-fields by solving the Poisson equation for the electrostatic field in the reference frame where the beam may be considered at rest, and then transforming the fields back to the laboratory frame where kicks to the particles are applied. TStep includes space-charge, the intrinsic/thermal emittance calculation and beam-loading and allows for 2D and 3D tracking calculations.

2.1.2 ASTRA

A Space charge TRacking Algorithm (`ASTRA`) tracks the particles through user defined external fields taking into account the space charge field of the particle cloud. The tracking is based on a non-adaptive Runge-Kutta integration of 4^{th} order. The beam line elements are set up w.r.t. a global coordinate system in `ASTRA`. All calculations in `ASTRA` are done with double precision, while output and input may be in single precision. The `ASTRA` code includes the space-charge and thermal emittance calculation and allows for 2D and 3D tracking calculations.

2.1.3 GPT

General Particle Tracer (GPT) is a completely 3D code, including the space-charge model. The equations of motion for the macro-particles are solved in the time-domain using a 5th order embedded Runge-Kutta integrator with adaptive step-size control. Optionally, the equations of motion are combined with additional differential equations. This mechanism can be used to calculate beam-loading or FEL interaction completely self-consistently.

2.1.4 RF-Track

RF-Track is a recent tracking code developed at CERN for the optimisation of low-energy ion linacs in the presence of space-charge effects. RF-Track can transport beams of particles with arbitrary mass and charge, even mixed together, solving fully relativistic equations of motion with a multitude of integration algorithms. It implements direct space-charge effects through a full 3D PIC implementation. RF-Track is written in parallel C++, and it uses the scripting languages Octave and Python as user interfaces.

Beside our studies, these tracking codes have been widely and successfully compared [18, 19] and validated with experimental results [20–22]. All the simulation codes mentioned above are capable of modelling RF photoinjectors, linacs, and XFEL beamlines (excluding undulators). There are also several differences between the codes, some of which are listed in a short comparison of code features shown in Table 3.

Table 3: Some Features of Space Charge Simulation Codes.

Code	TStep	GPT	ASTRA	RF-Track
Runs on Windows	Yes	Yes	Yes	No
Runs on Mac	No	Yes	Yes	Yes
Runs on Linux	No	Yes	Yes	Yes
Open Source	No	No	No	Yes
3D SC Algorithm	Yes	Yes	Yes	Yes
Adaptive Time steps	Yes	Yes	No	Yes
1D CSR Algoritm	Yes	Yes	No	No
Wakefield Algorithm	Yes	Yes	Yes	No
Scripting	No	No	No	Yes

2.2 Main Accelerating Section

One of the challenging problems to do with accelerating intense bunches in X-Band structures is the instability driven by wakefields. The wakefields are generated by a charged particle beam interacting with the vacuum chamber components. These components may have a complex geometry: kickers, bellows, RF cavity, diagnostics components, special devices, etc. To solve Maxwell's equations in a given complex structure, with the beam current as the source of fields, a study of the field is required. For this complicated task, dedicated computer codes were developed to solve the electromagnetic problem in the frequency or in the time domain. The theories for wakefield imply that the amplitude of the wakefield potential induced by the interaction between charged particles and vacuum chamber is inversely proportional to the geometric dimensions of the vacuum chamber. In other words, a smaller vacuum chamber dimension induces a higher wake potential.

For the transverse case, the wakefield instability is generated by off-axis beam trajectories. The instability develop within a single bunch or along a train of bunches. As the beam traverses the linac, the head of a single bunch (or first bunch of a train) undergoes an unperturbed transverse motion. The tail (or remaining bunches of the train), on the other hand, experiences deflection due to the wake excited by the preceding particles (bunches). The transvese wakefield instability always leads to emittance growth or beam losses. For the longitudinal case, on the other hand, the bunches (or tail of a single bunch) travelling through the linac will lose energy due to the longitudinal wakefields excited by preceding bunches (or preceding particles wihtin single bunch) independent of whether the bunches have off-axis trajectories. To minimise the emittance dilution, or especially to fulfill the small sliced energy spread requirement of the FEL (see Sec 3.3, the energy spread of the beam must be kept as small as possible.

The preservation of the beam emittance along the accelerator and transport lines is an important issue to achieve design XFEL performance. In a real, imperfect, machine the linac consists of randomly misaligned accelerating sections which cause deflection of the particles at the tail by the transverse wakefield induced by the leading particles. Or, due to injection transverse jitter, the beam performs coherent betatron oscillations down the linac leading to chromatic and wakefield emittance dilution. The chromatic emittance dilution in turn is conditioned by residual uncorrelated energy spread after the bunch compressor and correlated energy spread. Longitudinal wakefields modify the correlated energy spread, while the transverse wakefields induced by off-axis beam motion disturb the transverse shape of the bunch. As a result, the particles of the bunch are diluted in a single slice (uncorrelated, chromatic) and within the bunch (correlated, chromatic and wakefield).

Since the FEL mechanism requires high peak current, it necessary to design magnetic bunch compressors on a machine like CompactLight which increase the peak current while maintaining the small emittance. However one of the major problems with the acceleration of ultra-short electron bunches is Coherent synchrotron radiation (CSR). Studies in the past show that the CSR can cause emittance growth in bunch compressor chicanes [23]. Recent simulation studies and theoretical investigations have shown that such a bending system is subject to the microbunching instability driven by CSR and hence can be very sensistive to any energy density or energy modulation of the incoming beam distribution [24].

The simulation tool for optimizing the main accelerating section must be able to simulate all the problems mentioned above, as well as the other misalignments or imperfections in the machine. A flexible matching feature for the optics of the different sections is also important for long term iteration processes during the optimization. The simulation codes should provide the opportunity to design corrections for mitigating the effects of machine imperfections. CompactLight collaborators use several widely used and well established simulation codes for simulating all the effects. We have chosen `ELEGANT` and `PLACET` for the design of main accelerating section of the CompactLight.

In addition, one may need a fast optimization method to manipulate the longitudinal phase space of a single bunch. In order to reach kA-level peak current at multi-GeV beam energy with minimised energy spread, one needs to fine tune the longitudinal machine parameters in a reasonable time. One can optimize the longitudinal phase space without using the full 6-D phase space of the bunch. The key parameters of the accelerator and bunch compressors, such as compression factors and RF setup, are driven by the longitudinal evolution of the phase space along the machine. Since in most accelerators the longitudinal phase space can be studied independently of the transverse phase space, it can be advantageous to employ a program that tracks longitudinal coordinates only. Linear approximations of the beam dynamics are insufficient to fully represent the beam evolution. Several nonlinear effects have a leading role in shaping the final longitudinal bunch profile, for example: the non-linearity of the magnetic chicanes, usually referred to with the T_{566} and U_{5666} terms, the curvature due to the RF accelerating fields, the correlated energy spread introduced by short-range wakefields in the accelerating structures, the non-linearity of the distribution as it comes from the injector. Dedicated computer codes are necessary for this purpose. We have tested two such codes: `LiTrack`[8] and `Track1D`[9].

2.2.1 LiTrack

`LiTrack` is a fast Matlab-based 1D macroparticle tracking code suitable for the determination of the linac parameters, such as RF peak voltage and lengths, in order to accomplish the aforementioned tasks. Arbitrary short-range (i.e., single bunch) linac wakefields can be incorporated as external text files, treated as impedances (the charge distribution is assumed to be frozen during acceleration), and convoluted with the arbitrary longitudinal charge distribution. Bunch length compression in arbitrary magnetic insertions is described by means of user-defined linear and nonlinear (up to 3^{rd} order) momentum compaction terms. LiTrack can also be run from a Matlab script by calling it as a function. This allows the user, for example, to scan or randomise input parameters. LiTrack has been used in the last 20 years for the design of electron accelerators such as linear colliders and high gain FELs, for example the LCLS [25] at SLAC. It was applied to sensitivity studies in order to specify the jitter budget, and was benchmarked with 2D or 3D codes such as Elegant and IMPACT.

2.2.2 Track1D

`Track1D` is a fast C++ library embedded into `Octave` [26] which tracks 1D single-bunch distributions through linacs and magnetic chicanes. It implements single-bunch longitudinal wakefields in accelerating structures, as well as chicanes with adjustable R_{56}, T_{566}, and U_{5666}. Being embedded in Octave, it can easily be interfaced with the optimisation toolbox offered by this software. This permits multidimensional optimisation of the overall layout, using the relevant degrees of freedom, targeting non-trivial merit functions which can simultaneously address multiple goals: short bunch length, uniform current distribution, small sliced energy spread. It enables flexible output and plotting thanks to Octave. It typically runs 10^5 particles in fractions of a second.

2.2.3 ELEGANT

ELEctron Generation ANd Tracking (`ELEGANT`), which is written in the C programming language, is a full 6D particle tracking program. It uses a variant of the `MAD` [27] input format to describe accelerator components. Program execution is driven by commands in a namelist format. `ELEGANT` is not a stand-alone program. For example, most of the output is not human-readable, and `ELEGANT` itself has no graphics capabilities. These tasks are handled by a suite of post-processing programs that serve both `ELEGANT` and other physics programs. These programs, collectively known as the `SDDS-Toolkit` [28], provide sophisticated data analysis and display capabilities. They also serve to prepare input for `ELEGANT`, supporting multi-stage simulation.

ELEGANT is a matrix based tracking code up to third order for most of the elements. However it is also possible to track via canonical kick elements, numerically integrated elements, or any combination of all those. Like many accelerator codes, ELEGANT does accelerator optimization. It will fit the first- and second-order matrix, beta functions, tunes, chromaticities, natural emittance, etc. It also has the ability to optimize tracking results using a user-supplied merit function of the final beam and transport parameters.

2.2.4 PLACET

Program for Linear Accelerator Correction and Efficiency Tests (PLACET) is a code to simulate the dynamics of a beam in the main accelerating or decelerating part of a linac in the presence of wakefields, synchrotron radiation emission, misalignments and other imperfections. It allows investigation of single- and multi-bunch effects, and simulation of normal cavities with relatively low group velocities as well as the special transfer structures specific to CLIC. In these, the group velocity is a significant fraction of the speed of light (around 50%). A number of correction schemes allow testing the emittance growth to be expected for given pre-alignment errors. PLACET is written in parallel C and C++, and it uses the scripting languages Tcl/Tk Octave and Python as user interfaces.

The simulation codes to be used for the optimization of the main accelerating section are capable of modelling linacs, and XFEL beamlines (excluding undulators) with the existence of wakefield and CSR effects as well as misalignments and other imperfections. There are also several differences between the codes, some of which are listed in a short comparison of code features shown in Table 4.

Table 4: Some Features of Accelerator Simulation Codes.

Code	**LiTrack**	**Track1D**	**ELEGANT**	**PLACET**
Runs on Windows	Yes	Yes	Yes	No
Runs on Mac	No	Yes	Yes	Yes
Runs on Linux	No	Yes	Yes	Yes
Open Source	No	Tes	No	Yes
Adaptive Time steps	No	No	No	No
1D CSR Algoritm	Yes	No	Yes	Yes
Wakefield Algorithm	Yes	Yes	Yes	Yes
Scripting	No	No	No	Yes

2.3 Free Electron Laser Section

The FEL is a type of coherent light source, based on the amplification of radiation by a high-energy electron beam generated in an electron accelerator. The lasing mechanism of X-ray FELs can be described by classical electrodynamics. Even though there are several analytical formulas to describe the amplification process in FELs [29, 30], we usually need to perform numerical simulations to precisely quantify the light source performance available under practical conditions. During the 1980s a number of codes had been written, suitable for simulating the SASE process [31]. These codes have been used for the designs of the Linac Coherent Light Source (LCLS) and TESLA Test Facility (TTF) projects as well as for a number of long-wavelengths experiments.

To simulate the FEL process, the electron beam is typically divided into a number of slices, each the length of the radiation wavelength, along the longitudinal axis. For an X-ray FEL the number of slices required to cover the whole electron beam can be large so simulations can be time-consuming. For quick estimates of FEL performance semi-analytic methods can be used.

2.3.1 PROMETEO

`PROMETEO` is a multi-particle code for simulating FEL sources [32]. The code has been used both as a research tool to understand the dynamics of FELs operating in different configurations and as a practical tool to design FEL devices. It is a flexible tool that can deal with many FEL configurations, including optical klystrons and segmented undulators. The code can simulate the evolution of the fundamental and the coherent generation of higher-order harmonics in SASE or oscillator FELs. The code can model 1-dimensional effects like pulse propagation in FEL oscillators and in high-gain SASE devices, including spiking dynamics. In order to have a fast simulation capability, three-dimensional contributions from electromagnetic and electron beam propagation are deliberately omitted. The latter have been taken into account by including them as longitudinal effects. One of its important features is the development of a series of practical formulae aimed at providing a quick evaluation of the FEL performances, be it operating in the SASE, Oscillator or Optical Klystron mode.

2.3.2 PERSEO

`PERSEO` is a library of functions developed for the simulation of FEL dynamics within the Mathcad® framework [10, 33]. The core of the library consists of the routines solving the pendulum-like FEL equations coupled with the field equations that govern the FEL longitudinal dynamics, and including self-consistently the field variables for the higher order harmonics. `PERSEO` FEL-cad library allows the 1D simulation of SASE FEL configurations, oscillator configurations and exotic configurations like MOPA. It includes higher order harmonics and startup from shot-noise. Time dependent simulations can be programmed within Mathcad, and future extensions will extend the simulation to the transverse space. Detailed description of `PERSEO` is given in Section 3.3.1

2.3.3 GENESIS

`GENESIS` is a time-dependent three-dimensional FEL code [11, 12]. It can simulate single-pass free-electron lasers, both FEL amplifier and SASE FEL, and the flexible input can be used to extend the capability to FEL oscillators or multistage set-ups with higher harmonics. Its origin is the steady-state 2D code `TDA3D` but nowadays they have nothing in common except for some naming convention. The radiation field is discretized on a Cartesian grid and solved by the alternating direction implicit (ADI) integration scheme. The transverse motion of the electron beam, described by macroparticles, is calculated analytically, whereas the energy and phase are found by Runge-Kutta integration. In addition to the standard internal generation, an external seeding radiation field, undulator field, and longitudinal variation of the electron beam parameters can be supplied in input files. Long-term electro-static fields (e.g. wake fields) must be calculated externally. They can be implemented into GENESIS and applied to the equations of motion for the macro particles.

2.3.4 GINGER

GINGER is a 3D multi-frequency particle tracking code with a 2D, axi-symmetric representation of the radiation field [34]. The equations of motion are averaged over an undulator period. For non-waveguide simulations, GINGER uses a nonlinear, expanding radial grid, proportional to the square of the radius near the axis, and expands exponentially for large distances from the axis. The outer grid boundary, the number of radial grid zones, as well as the region over which the grid is linear, are controlled by input parameters. GINGER is able to simulate a single segment of undulator as well as lumped, quadrupole focusing.

There are several more codes, such as MEDUSA, TDA3D, RAD and PUFFIN [35], for simulating FELs, and most of them have already been bench-marked against other FEL simulation codes (such as: GINGER [36], FAST [37], MINERVA [38] and PUFFIN [35]) and theoretical predictions for different configurations and schemes (SASE [39], harmonic lasing using FAST and GINGER [40], HGHG and Echo-Enabled Harmonic Generation using PUFFIN [41]) providing a good agreement in the FEL figures of merit.

A more detailed description and comparison of the codes to be used for the optimization of the FEL section is given in Section 3.3. The main differences between the codes are summarized in Table 5.

Table 5: Some Features of Free Electron Laser Simulation Codes.

Code	**PROMETEO**	**PERSEO**	**GENESIS**
Runs on Windows	Yes	Yes	Yes
Runs on Mac	Yes	No	Yes
Runs on Linux	Yes	No	Yes
Open Source	Yes	No	Yes
Radiation Field	1D	1D	3D
Wiggler Errors	No	No	Yes
Wakefield Algorithm	No	No	Yes
Scripting	No	No	Yes

2.4 The units to be used for exchange of results

In order to use all the codes mentioned above we need to develop a systematic way to transfer results between existing and possible future codes. The exchange tool shall provide a common, generalized pre- and post-processing facility for simulations. It could also include graphics features as well as scripting, permitting a high degree of automation. Because of the scope of the simulations, it is possible to employ a distributed batch queue of workstations. Job preparation, submission, and post-processing, as well as inter-job data transfer, could be performed using scripts, eliminating the tedium and errors implicit in less automated data handling.

Beam distribution files from various codes may consist of a header giving information about the contents of the file, while some of them start only with an array of data for the 6-D phase space coordinates of the particles. The translator shall also be used to analyze the statistical properties for the beam or Twiss parameters. Table 6 lists the structure of particle distribution files of 6D simulation tools to be used for CompactLight. The last column of the table shows the units for the file exchange between codes.

Table 6: Phase space coordinate descriptions for the 3D simulation tools

Quantity	`TStep`	`GPT`	`ASTRA`	`RF-Track`	`ELEGANT`	`PLACET`	`GENESIS`	**Translator**
x-position (x)	cm	m	m	mm	m	μm	m	mm
x-momentum (x')	rad	$\gamma\beta_x$	eV/c	mrad	p_x/p_z	μrad	$\gamma\beta_x$	MeV/c
y-position (y)	cm	m	m	mm	m	μm	m	mm
y-momentum (y')	rad	$\gamma\beta_y$	eV/c	mrad	p_y/p_z	μrad	$\gamma\beta_y$	MeV/c
z-position (z)	degree	m	m	mm	m	μm	m	mm
t-position (t)	degree	s	s	mm/c	m/c	μm/c	s	ps
Total momentum (P)	MeV/c	$\gamma\beta$	eV/c	MeV/c	$\gamma\beta$	GeV	$\gamma\beta$	MeV/c
Energy (E)	MeV	γ	eV	MeV	γ	GeV	γ	MeV

3 Comparison of codes

In accordance with the project implementation plan, different electron gun schemes at different operating frequency (S, C and X band) have been investigated by WP3. WP3, on the other hand, is exploring the possibilities for phase-space linearization and compression schemes based on the injector choice. Considerable progress has been made on RF structure design and module layout by WP4. Based on the user demands defined by WP2, the technology of undulator design is being investigated by WP5. In order to provide the key parameters and performance estimates of the machine and elaborate the overall facility design we aim to develop and apply consistent tools for modelling the machine from the cathode to the undulator exit by using available simulation tools.

The simulation codes which are going to be used for WP6 are briefly summarized in Section 2. To test the tools we have considered the sections of CompactLight independently instead of focusing on a layout of the whole facility. The codes could not have been integrated because of too many options for the injector and bunch compressor schemes. On the other hand the codes somehow could be bench-marked for the specific task of interest. The following specific tasks were considered to compare and evaluate the codes:

- Injector up to 300 MeV, comprising an S-Band RF-Photo-cathode gun and S-band travelling wave RF structures: `ASTRA`, `GPT`, `TStep` and `RF-Track` codes are compared
- Main linac up to 6 GeV comprising X-Band travelling wave RF structures and two bunch compressors: In addition to the comparison between `ELEGANT` and `PLACET` codes, 2D codes `LiTrack` and `Track1D` codes are used.
- Hard X-Ray beamline comprising a planar undulator suitable for producing 0.7 Å (16 keV photon energy) FEL output: Semi-analytical formalism (Ming Xie and Dattoli et al.) and time dependent `GENESIS` and `PERSEO` codes are compared

3.1 Comparison of Injector Simulation Tools

Different simulation tools have been used to optimise the beam dynamics in the photo-injector to compare the different resolution approaches that the codes adopt and to state the reliability of the simulation results that will guide the machine design. The codes have been chosen for their abilities in treating space charge effects experienced by the low energy electron beam from its generation at the cathode up to the linac entrance, and the beam emitting from the cathode surface that strongly impacts the intrinsic emittance with which the beam is generated and that represents the best emittance one can obtain at the FEL injection.

As mentioned in Section 2.1 the beam dynamics in the photo-injector has been simulated with three well established tools for the study of charged particle dynamics in electromagnetic fields i.e. `TStep`, `ASTRA` and `GPT`. We also tested a new code that was developed at CERN over the last few years, `RF-Track`.

3.1.1 Simulation setup

The simulation has been performed on a setup comprising an S-band photo-injector, operating at 2.856 GHz followed by 3-meter long SLAC-type travelling wave (TW) sections operating at 2.856 GHz [42] (See Fig. 2). The layout consists of a 1.6 cell Standing Wave (SW) RF gun, equipped with a copper photo-cathode and an emittance compensation solenoid. The first two accelerating sections are embedded in solenoids for operation in velocity bunching mode. Each solenoid is composed of twelve coils grouped in four coils with each group independently supplied.

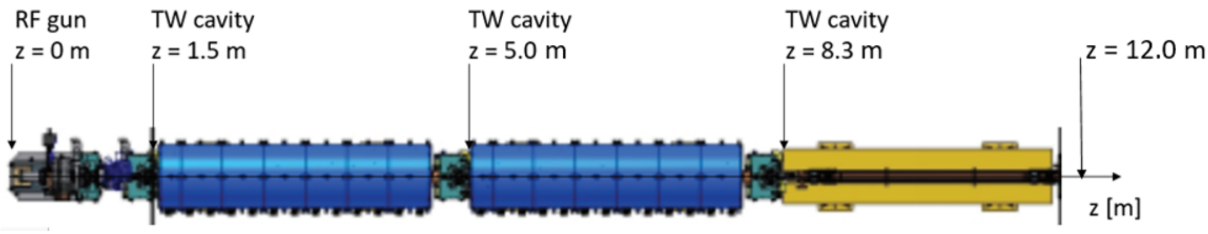

Figure 2: Layout of the SPARC-like high brightness S-band photo-injector consisting of a 1.6 cell UCLA/BNL type SW RF gun, equipped with a copper photo cathode and an emittance compensation solenoid, followed by three TW SLAC type sections; two compensation solenoids surround the first and the second S-band cavities for operation in the velocity bunching mode.

The RF gun and its solenoid are the ones designed for the ELI-NP GBS facility [43] and are well described in [44]. The solenoid is composed of two coils independently powered and it is placed at 204 mm from the cathode surface. The SLAC-type travelling wave sections are composed of 84 cells with 2/3π phase advance per cell and 56.7 MΩ/m shunt impedance.

A TW cavity is composed of a TW central body and input and output couplers. The central body consists of n TW cells with a 2π/3 field phase advance per cell (with $n = 1\ldots$ncell, and ncell the total cell number in the structure) to provide a good enough approximation to the design gradient profile. The input and output couplers consist of pure π-mode standing wave cells according to the Serafini-Rosensweig model described in [45]: the fringe fields at both sides of the TW cavity are simulated with a half standing wave cell. The reason why it is important to include the couplers in the model lies in the transverse focusing strength provided by a pure π-mode standing wave structure, which is $K_r = \frac{1}{8}(\gamma'/\gamma)^2$ (whereas for TW accelerating cells it disappears completely).

Differences between the codes and their peculiarities will be treated in more details below, focusing on space charge routines and the modelling of the intrinsic emittance and the travelling wave cavities.

Space charge algorithms: The space charge routines implemented in the codes have been carefully investigated, the space charge force being mainly responsible for the emittance dilution of the electron beam in this part of the machine. Space charge calculations can be performed relying on 2D mesh rings (if the cylindrical symmetry is assumed) or a fully 3D mesh grid. In the former, cylindrical mesh rings are set up with the beam composed of concentric rings of constant charge density and longitudinal slices; in the latter a cubic mesh grid is set up that covers the entire beam in a point-to-point model. Even if the ASTRA and TStep codes enable the user to perform 3D simulations, their manuals strongly recommend using it with care since in both cases the point-to-point calculation might be noisy if the number of macro-particles is not sufficient. The results are generally accurate when using >100k macro-particles at the expense of increasing considerably the computer time. However, the required number of particles might depend on the case under study. Furthermore, the 3D space charge routines implemented in TStep may underestimate the radial space charge force at high energy, if the number of particles is too low, while the one implemented in ASTRA does not provide special features for tailoring the emission of particles from the cathode and the image charge forces cannot be included. On the contrary, the default GPT space charge calculation is based on a 3D mesh grid model so it is powerful and able to keep the computing costs to a minimum without compromising the accuracy.

Emission process and intrinsic emittance: The emission of a beam from a photo-cathode is a complex phenomenon and may be determined by the interaction between various factors such as the set-up of the laser pulse and accelerating field, the cathode features and many other mechanisms—for example the image charge and the space charge fields, the Schottky effect and the quantum efficiency. The chosen codes are able to simulate a pseudo-realistic distribution of a beam emitted from a cathode. The image and space charge fields are included in the calculations, but the physics involved in the electrons' generation are not.

In a typical RF photo-injector the electron beam is emitted from a copper or semiconductor cathode surface illuminated by a laser pulse when the applied RF accelerating field overcomes the electric field produced by the electron bunch itself—image and space charge fields. Indeed, the electrons experience their own image charge, which for metal cathodes, produces a field opposing the applied electric field. The codes calculate the image charge field at the cathode by assuming a metal wall (Dirichlet boundary condition) and add it to the bunch self-field; the calculation is turned-off at a distance from the cathode where the image charge field contribution on the overall fields becomes negligible (for example because of a long distance between beam and cathode).

The bunch generation is a time-dependent process determined, at the first order, by the laser pulse distribution. In addition, during and immediately after the emission, the space charge pressure on the beam will lead to a very fast change in the beam length and the transverse size. The time step increment and the space charge mesh adjustments are then the main issues to be faced in the cathode area in order to ensure sufficient accuracy of the simulation. The adopted codes foresee a dynamical set-up of the grid, to closely match the actual beam dimensions, and an adaptive time-step, that scales with the beam length and γ. The accuracy of the calculation can be improved by the user by increasing the number of the longitudinal slices and rings (`TStep` and `ASTRA`) or of the grid meshes (`GPT`), and both `ASTRA` and `GPT` permit to vary the volume of the rings or grid meshes according to the bunch charge density in order to avoid statistical fluctuation in the case of rarely populated meshes. In detail, `ASTRA` enables the user to vary the radial grid height over the bunch radius and to merge the slices if needed (useful in the case of long and low density tails) while `GPT` relies by default on an adaptive meshing technique that optimises the number and the thickness of the grid mesh based on the charge density distribution.

Finally, in a photo-injector the beam is generated at the cathode with its own intrinsic emittance. The treatment of this parameter in the codes is based on analytic models widely described in the literature [46, 47] and it is a key output of the simulation since it will represent the lowest emittance value one can get at the FEL injection. In general, the electrons extracted from a metal cathode belong to the tail of the Fermi-Dirac distribution and have the Maxwell velocity distribution given by

$$f\left(v_x, v_y, v_z\right) = f_0 \exp\left(-\frac{m\left(v_x^2+v_y^2+v_z^2\right)}{2k_BT}\right) \tag{1}$$

where k_B is Boltzmann constant and T the cathode temperature. The result is that, according to [47], the particles emerging from the cathode at room temperature have an intrinsic velocity spread and so an intrinsic emittance described as

$$\varepsilon_{x,y}^{\text{intrinsic}} = \sigma_{x,y}\sqrt{\frac{E_{\text{phot}}-\Phi_{\text{eff}}}{3m_0c^2}} \tag{2}$$

where $\sigma_{x,y}$ is the rms beam size, Φ_{eff} is the effective work function and E_{phot} is the photon energy. This is the model implemented in `ASTRA`, which is also the only code that explicitly foresees the treatment of the Schottky effect.

An alternative model, implemented in `ASTRA`, `TStep` and `GPT`, foresees a beam distribution with isotropic emission angles into a half sphere over the cathode according to [46] with the intrinsic emittance being

$$\varepsilon_{x,y}^{\text{intrinsic}} = \sigma_{x,y}\sqrt{\frac{2E_{\text{kin}}}{3m_0c^2}} \tag{3}$$

where E_{kin} represents the beam kinetic energy. In particular, the `TStep` code first makes each particle direction perpendicular to the cathode surface with rest mass energy and then applies random momentum changes corresponding to E_{kin}. In addition, `GPT` gives the possibility to set a user-defined value for the initial beam emittance just by scaling linearly the transverse momentum.

3.1.2 Simulation of Injector

Several configurations have been proposed for the XLS photo-injector, aiming to provide at the linac entrance an electron beam with 50-100 pC charge, less than 0.4 mm-mrad projected emittance and less than 300 μm bunch length. In this section we will adopt as reference for the code benchmarking the case of a 100 pC beam generated in a SPARC-like S-band photo-injector [48] and delivered at the linac entrance with a final energy of 140 MeV, a normalised projected emittance of 0.6 mm-mrad and a bunch length of 350 μm (all values are rms quantities).

The working point has been chosen to be close to the likely point required from the FEL community. Nevertheless, it does not represent the final beam injection requests since for the benchmark simplicity a uniform laser pulse transverse distribution and a 100 MeV beam exiting the photo-injector have been considered. Instead the choice of the machine layout has been instead guided by the expertise acquired on the S-band technology that ensures a very good agreement between the simulated and measured field maps for the beam-line elements.

Input particle distribution: As mentioned, for the benchmark procedure, the choice has been to adopt a photo-cathode laser pulse with a Gaussian longitudinal profile of σ_z=30 μm (100 fs RMS) duration and a transverse uniform distribution with σ_r=250 μm and radius r = 0.5 mm. The intrinsic emittance of such beam at the cathode, determined by the codes as illustrated in eq. 3, is about 0.6 [mm-mrad/mm]$\sigma_{x,y}$[mm], i.e. $\simeq$ 0.15 mm-mrad.

Figure 3 shows the shaped charge distribution at the cathode surface produced by such a laser pulse as obtained with 2D `TStep` simulations.

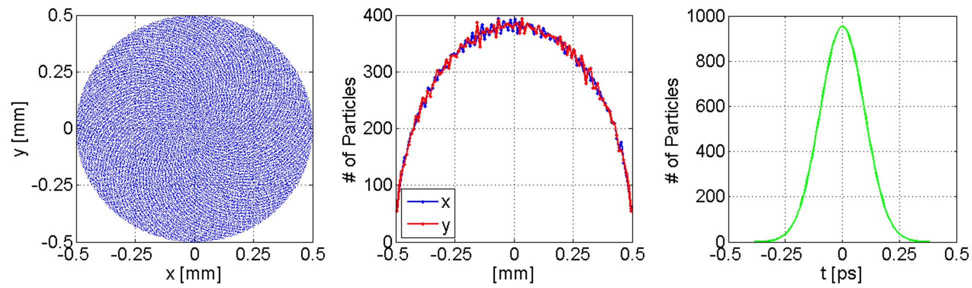

Figure 3: Charge distribution at cathode surface produced by the photo-cathode laser pulse as obtained with 2D TStep simulations.

Rather than generating the initial particle distribution internally, the tracking programs can also read the initial particle coordinates from a file. This file may be generated by the program `generator` or by a user written program based on the emission theory.

Space charge mesh: With the assumption of cylindrical symmetry, here the choice has been to adopt the 2D model for `ASTRA` and `TStep` simulations and the 3D model for `GPT`, trying to optimise the code performance and accuracy. The beam has been modelled with 30k macro-particles, which represents a good compromise between reliability and computational time for all the codes and that suffices if one is interested in the beam projected quantities (for example the emittance or energy spread). Actually, many more macro-particles (>100 k) would be needed if one was interested in the beam slice parameters or needed to study phenomena such as, for example, the longitudinal micro-bunching instability.

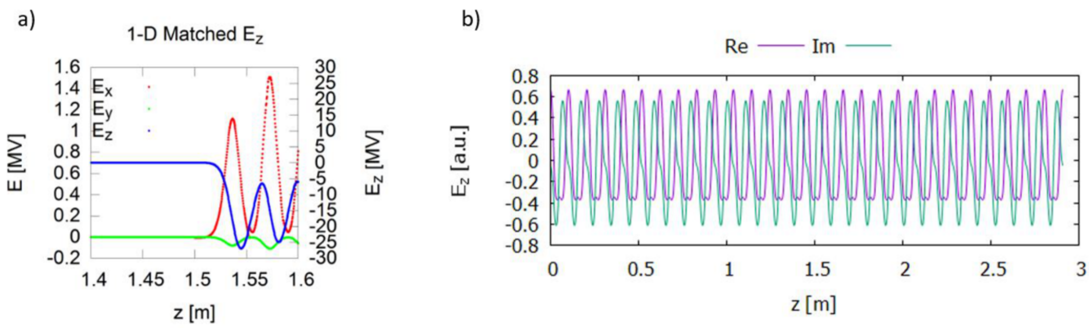

Figure 4: The electromagnetic field for the TW sections as obtained by GPT simulations (and similarly by ASTRA and TStep): the Fig.4 a) illustrates the transition between the input coupler and the first travelling wave cell; the Fig.4 b) illustrates the electromagnetic field in the body of the TW section.

Input fields: The beam-line elements have been implemented in the codes with field maps obtained by means of `SUPERFISH` (electromagnetic for accelerating cavities) and `POISSON` (magneto-static for solenoids) simulations. The electromagnetic field for the TW sections for `GPT` is created by combining the real and imaginary parts of the `SUPERFISH` solution of the cavity, as described in [49]. Figure 4 shows the on-axis field components used in simulations:

Fig.4 a) illustrates the transition between the input coupler and the first travelling wave cell; the Fig.4 b) illustrates the electromagnetic field in the body of the TW section.

The implementation of TW fields is performed combining SW and TW cavities by default both in `ASTRA` and in `TStep`, while a user-defined element can be defined in `GPT` according to the expected field-map from the cavities. A fine tuning of the phase and amplitude of the couplers and of the body cells is crucial to avoid any abrupt field discontinuity.

The injector has been simulated with all the appropriate codes. The parameter setup, from the beam dynamics optimisation by means of `TStep` simulations, is summarised in Table 7. Similar parameters were also obtained by other codes with minor difference of cosine and sine wave convention.

Table 7: Summary of the photo-injector setup, as it results from the beam dynamics optimisation by means of TStep simulations.

Section	**Parameter**	**Unit**	**Value**
RF Gun	Electric field amplitude	MV/m	120
	Solenoid magnetic field	kG	3.2
	RF operation phase	deg	≃24
	Output beam energy	MeV	6.5
TW sections ($1^{st}/2^{nd}$)	Electric field amplitude	MV/m	20.0/25.0
	Solenoid magnetic field	kG	0
	RF operation phase	deg	0.0/-11.3

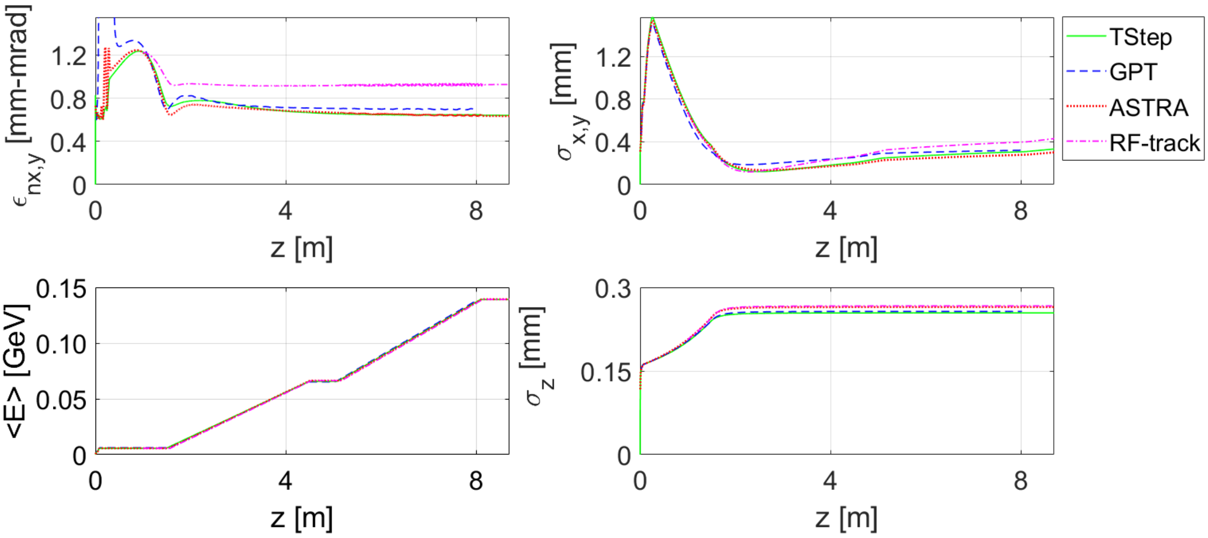

Figure 5: Evolution of the electron beam parameters along the photo-injector as obtained by `TStep` (green line), `ASTRA` (red dots) and `GPT` (blue dashed line). All values are rms quantities.

The beam line matching foresees a proper set of emittance compensation solenoids and of the S-band cavity gradients, according to the invariant envelope criteria [50]. In this configuration the first TW section can operate both on crest or far from the crest, in the velocity bunching regime [51], enabling the RF compression of the beam length, while the following section operates almost on crest in order to let the electron bunch gain the maximum energy available in the TW cavities and freeze its phase space quality.

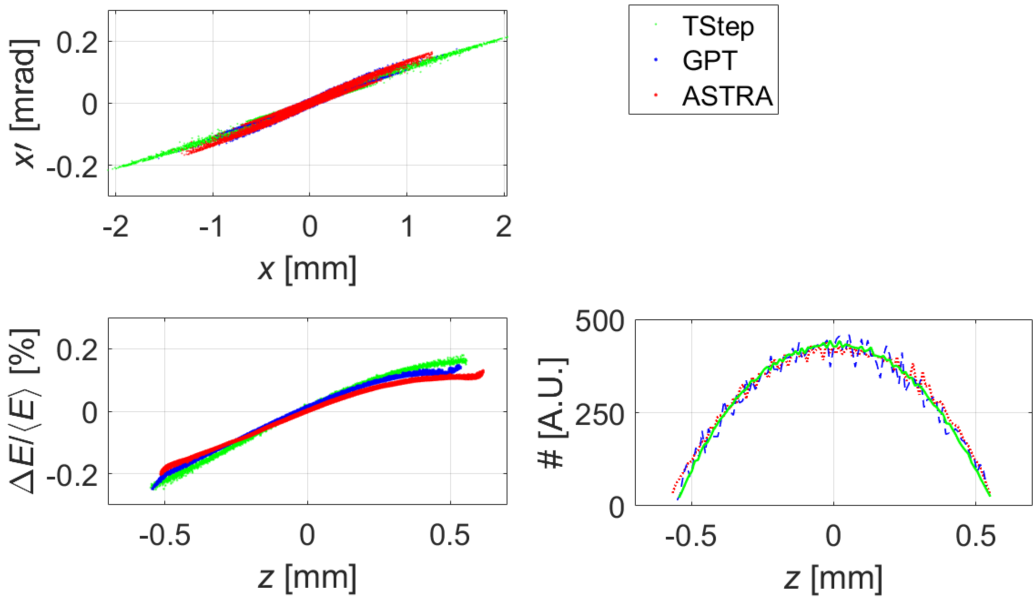

Figure 6: Phase-space portraits at the photo-injector exit

Figure 5 shows the evaluation of rms beam parameters along the injector for various simulation codes. As clearly shown the codes have good agreement. Figure 6 shows the transverse and longitudinal phase space of the single bunch obtained by `TStep`, `ASTRA` and `GPT`. As easily can be seen `ASTRA` and `GPT` have good agreement for all phase spaces while `TStep` shows small differences in transverse phase space.

The results illustrated do not show relevant discrepancies between `TStep`, `ASTRA` and `GPT` simulations once one implements the same field maps and initial distributions at the cathode surface. The main difference lies in the gun region and it is related to the operating phase of the RF gun. Indeed, some tuning of the RF gun operating phase is needed in `GPT` simulations in order to reproduce the same beam evolution in the gun region obtained by `ASTRA` and `TStep`which completely agree. This behaviour can be explained by the different algorithms modelling space charge forces in the codes as illustrated in 3.1.1. Our thesis is supported by the fact that in the gun region the electron beam expands very fast due to the space charge pressure. Further, in the drift upstream of the first TW section the beam length as obtained by `ASTRA` increases faster than the length obtained by `GPT` and `TStep` leading to a 10 μm longer beam, corresponding to a $\simeq$ 3% variation. On the other hand, `ASTRA` and `TStep` are in excellent agreement if one looks at the evolution of the transverse emittance while `GPT` shows some discrepancies arising inside the TW sections leading to a $\simeq 6\%$ larger emittance.

As mentioned, we also tested the `RF-Track` code. The code does not yet implement the emission process from the cathode and, because of that, some discrepancies arise if one turns-on the space charge calculation in the cathode region. This limitation has been solved by tracking the beam distribution, obtained by means of ASTRA simulations, from downstream the RF gun. The `ASTRA` output file "PROJECTNAME.Cathode.001" is related to this process. In fact, as stated in [2], Table 4, this file contains the "longitudinal space-charge field on cathode

V/m" and the "accelerating field on cathode V/m".The implementation of the emission process in the RF−Track will be investigated further in the near future. The results are illustrated in Figure 5 with the RF−Track code in agreement with the other ones, especially in the longitudinal beam phase space.

The final beam parameters as obtained by simulations are listed in Table 8.

Table 8: Output beam parameters.

Beam Parameter	**TStep**	**GPT**	**ASTRA**	**RF−Track**	**Unit**
Charge	100	100	100	100	pC
Kinetic energy	139.6	139.9	139.3	139.2	MeV
Energy spread	0.10	0.09	0.09	0.11	%
RMS bunch length	254	256	264	266	μm
RMS normalized emittance	0.64	0.68	0.63	0.93	mm mrad
RMS size, $\sigma_{x,y}$	375	330	301	431	μm

3.1.3 Concluding & remarks

In this section we presented in details the ASTRA , TStep , GPT and RF−Track codes used for the design of the RF photo-injector. All these codes have been chosen for their specific capability in treating the beam dynamics in the low energy regime, where the space charge force is not negligible, and the emission process of an electron beam from a photo-cathode. Further these tracking codes have been widely and successfully compared and validated with experimental results. From the report it comes out that the main difference between the codes lies in the space charge algorithm, with GPT enabling for 3D space charge calculations without compromising the accuracy and elongating the time of the simulation. Beside this variation, the benchmark results have shown that all the codes are in agreement between them and with the analytical theory if one implements the same field maps and initial distributions at the cathode surface.

Finally RF−Track , a new code that was developed at CERN, has been tested. The results have shown that the code is in agreement with other codes, unless for the model of the space charge during the emission process near the cathode. Nevertheless, the RF−Track code still presents some advantages being it open source and not licensed and foreseeing parallel calculations that is in general a quite powerful and fast device.

3.2 Linac and bunch compressor simulation

Two simulation tools have been chosen for the linac simulations: ELEGANT[6] and PLACET[7]. Both are matrix-based codes that implement full 6D tracking and include collective effects relevant to the CompactLight project, such as wakefields in the accelerating structures and incoherent and coherent synchrotron radiation emission in the bending magnets. They can simulate bunch compressors as well as other elements like quadrupoles, accelerating structures, and compression chicanes.

Both codes have acquired a solid reputation in the field of linear accelerator and FEL simulation, and have successfully passed extensive benchmarks both against other codes and against experimental results, as it can be easily found in literature, for example [52].

3.2.1 Wakefield effects in the XLS accelerating structure

A knowledge of the short-range wakefields in the X-band accelerating structures is of critical importance for the design. The short-range longitudinal wakes both increase the single-bunch energy spread and introduce correlated energy spread; the short-range transverse wakes, in presence of structures' misalignment and/or orbit errors, increase the single-bunch projected emittance of the beam. The definition of misalignment tolerances depends on the effect of the wakefields. Our CompactLight simulations are based on the model described in [53]. This model defines an analytic expression of the wake potentials in terms of the geometry of the cell: its length, iris aperture, and gap length, as shown in Fig. 7. Table 9 reports the numbers as defined by WP4.

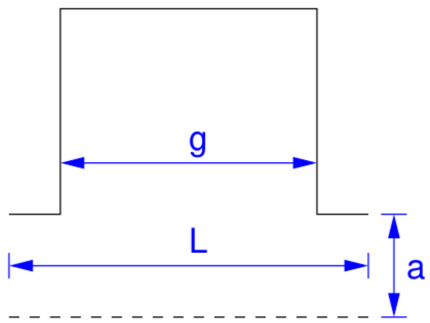

Figure 7: Cell parameters needed to compute the short-range longitudinal and transverse wakefields in the X-band accelerating structures: cell length L, iris aperture a, and gap length g.

Table 9: The XLS structure parameters used for wakefield calculations, as defined by WP4.

Parameter	Value	Description
$\langle a \rangle$	3.5 mm	average iris aperture
g	6.3 mm	gap length
L	8.3 mm	cell length

The simulation of the wakefields is similar in the two codes: an histogram of the arrival time is taken at the wakefield source, and it is convoluted with the wake potential in order to compute both the transverse and the longitudinal effect of the wake on each particle in the beam. The only difference between the two codes is that `PLACET` takes the single-particle wake function normalised to the element length, whereas `ELEGANT` takes the integrated wake function.

3.2.2 Simulation of synchrotron radiation emission

Synchrotron radiation emission in dipole magnets is of crucial importance in the design and performance optimisation of the linac and bunch compressors. Depending on the bunch length and energy, synchrotron radiation can be emitted either incoherently (ISR) or coherently (CSR). Synchrotron radiation emission is coherent when

$$\log_{10}(\sigma_z/\sigma_0) \leq 6.5,$$

where $\sigma_0 = R/\gamma^3$, with R the bending radius and γ the beam's relativistic factor [54].

In the incoherent regime all the electrons of the bunch emit photons independently from each other. This introduces into to the bunch uncorrelated energy spread, an average energy loss, and a transverse emittance growth. When the bunches are short and their energy is low, the photon emission can become coherent. In such a case, the coherent radiation can introduce a correlated energy spread and a significant emittance growth. CSR can also induce micro-bunching instability. An accurate simulation of these two regimes is therefore crucial.

Both `PLACET` and `ELEGANT` implement ISR and CSR. The model of ISR is very similar. It is based on random photon emission through quantum excitation. The CSR models are also similar, both being based on the the work of [23]. This model uses a 1D CSR kick and can correctly calculate the transient build-up of the CSR in bending magnets, however doesn't take into account shielding due to the beam pipe walls. `PLACET` implements CSR with shielding from the beam pipe walls.

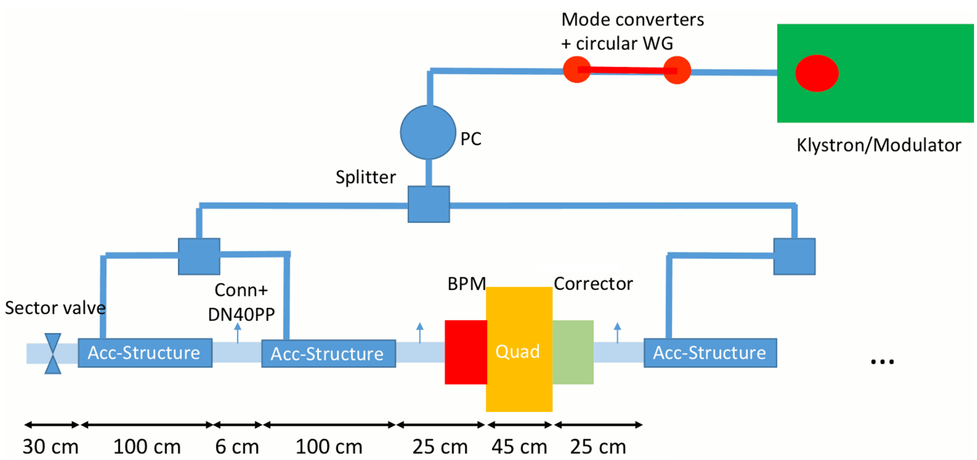

Figure 8: A sketch of the linac module considered in the code benchmark.

3.2.3 Simulated setup

Given that a well-defined lattice for CompactLight is not yet defined, the linac lattice was based on a sequence of FODO cells complying with preliminary module specifications provided by WP4. Each module coincides with an RF powering unit equipped with four accelerating structures, powered by a klystron with pulse compressor, and two quadrupoles. Each quadrupole is equipped with a BPM and a dipole corrector. A sketch of the module is shown in Fig. 8, where one can see the power distribution system and the expected dimensions of the elements. The linac accelerates the beam from an energy of 100 MeV up to an energy of 6.1 GeV, and two bunch compressors, located respectively at 300 MeV and 2.3 GeV, compress the bunches from 800 μm down to 10 μm. The linac between BC1 and BC2 is called linac1, the linac downstream of BC2 is called linac2. Figure 9 shows a sketch of the beamline used in the simulation.

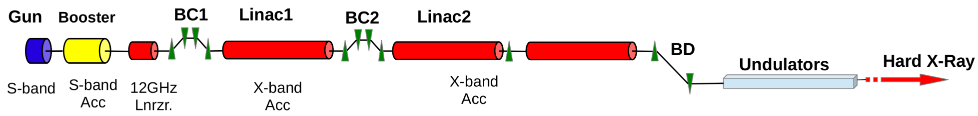

Figure 9: A sketch of the facility layout for simulation

3.2.4 Simulation results

Full 6D tracking was performed along the system using both ELEGANT and PLACET. A comparison of the results is shown in Fig. 10 and 11. Both code computes the Twiss functions along the beamline using matrix formalism thus there is good agreement between codes for Twiss functions. On the other hand, the transverse beam sizes $\sigma_{x,y}$ and average beam energy are computed using tracked beam distributions at the end of each beamline element. As can be seen in Figure 10 there is also good agreement for the transverse beam size and energy gain along linac.

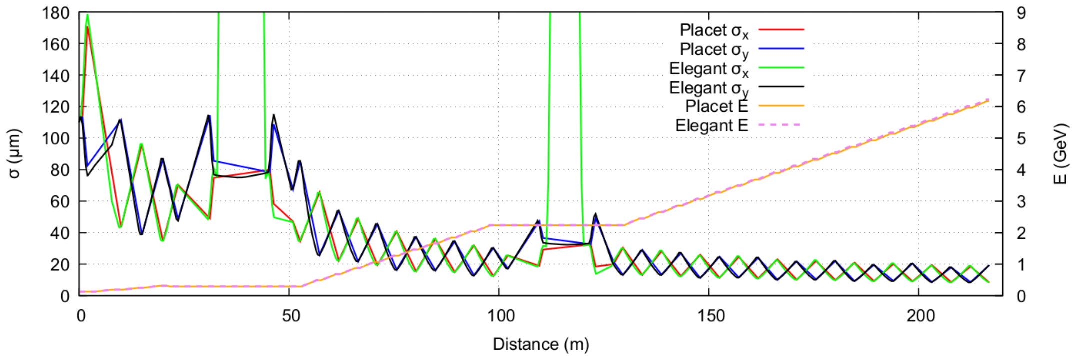

Figure 10: RMS transverse beam size along the lattice and the average beam energy, as returned by ELEGANT and PLACET.

Figure 11 shows the evaluation of phase spaces for different locations in the beamline. It can be noticed that a small discrepancy in the phase spaces produced by the two codes grows along the machine. This might be due to two reasons: the implementation of the wakefield effects, which depends on the algorithm parameters; and the fact that ELEGANT normalises the strength of the magnetic elements to the nominal energy profile, whereas PLACET adjusts automatically the magnetic strength of the magnets to the actual energy profile of the beam, which differs from the nominal profile due to the energy loss induced by longitudinal short-range wakefields and synchrotron radiation. Overall there is good agreement between codes and oce can match the phase spaces by fine tuning of the optic elements.

3.2.5 Optimization of longitudinal parameters

The initial design of an RF linear accelerator (linac) suitable to drive an X-ray FEL often relies on the manipulation of the electron beam longitudinal phase space. This has to be squeezed in time, in order to reach typically kA-level peak current, maximised in mean energy at multi-GeV level, and minimised in relative energy spread, often in the 0.%-0.01% range. To define the compression factors in bunch compressors (i.e. R_{56} of BCs) and RF setup (i.e. gradient

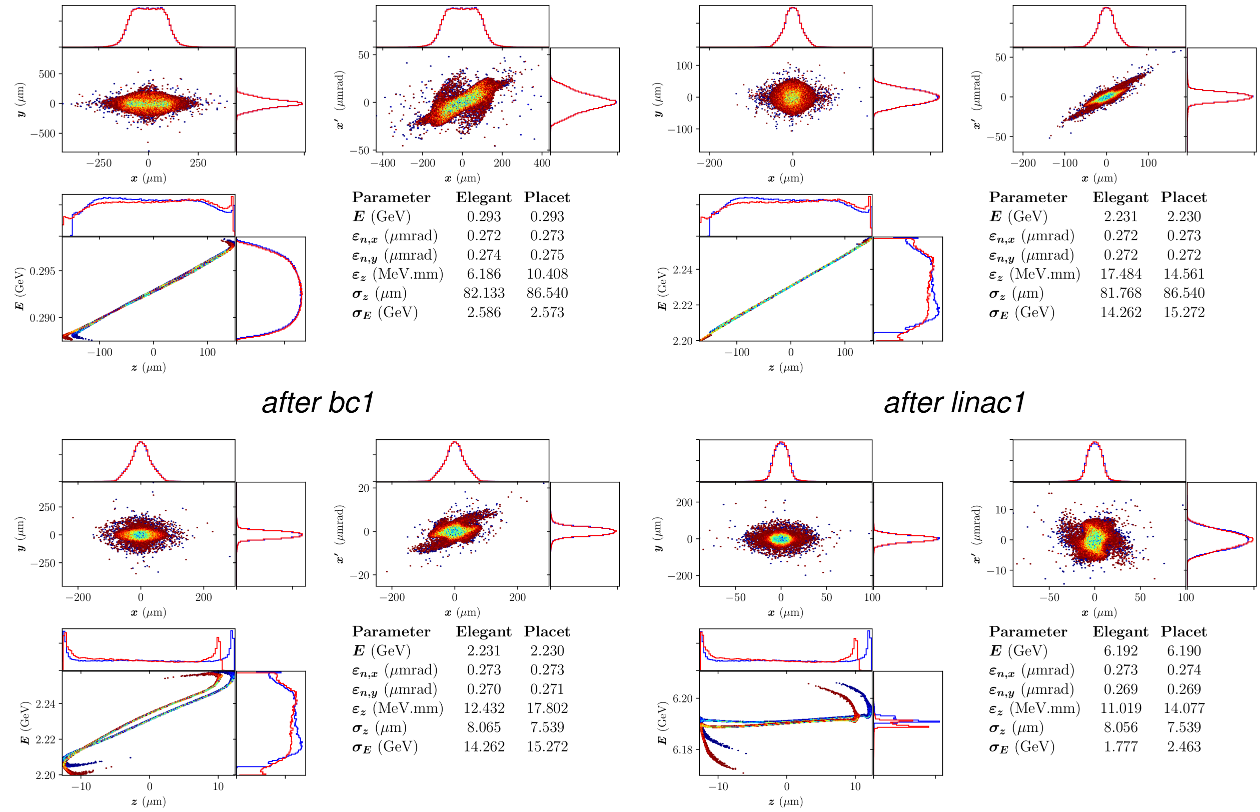

after bc1

Parameter	Elegant	Placet
E (GeV)	0.293	0.293
$\varepsilon_{n,x}$ (μmrad)	0.272	0.273
$\varepsilon_{n,y}$ (μmrad)	0.274	0.275
ε_z (MeV.mm)	6.186	10.408
σ_z (μm)	82.133	86.540
σ_E (GeV)	2.586	2.573

after linac1

Parameter	Elegant	Placet
E (GeV)	2.231	2.230
$\varepsilon_{n,x}$ (μmrad)	0.272	0.273
$\varepsilon_{n,y}$ (μmrad)	0.272	0.272
ε_z (MeV.mm)	17.484	14.561
σ_z (μm)	81.768	86.540
σ_E (GeV)	14.262	15.272

after bc2

Parameter	Elegant	Placet
E (GeV)	2.231	2.230
$\varepsilon_{n,x}$ (μmrad)	0.273	0.273
$\varepsilon_{n,y}$ (μmrad)	0.270	0.271
ε_z (MeV.mm)	12.432	17.802
σ_z (μm)	8.065	7.539
σ_E (GeV)	14.262	15.272

after linac2

Parameter	Elegant	Placet
E (GeV)	6.192	6.190
$\varepsilon_{n,x}$ (μmrad)	0.273	0.274
$\varepsilon_{n,y}$ (μmrad)	0.269	0.269
ε_z (MeV.mm)	11.019	14.077
σ_z (μm)	8.056	7.539
σ_E (GeV)	1.777	2.463

Figure 11: Phase-space portraits at four different locations along the machine.

and phase of all cavities) one can use 2D codes in which the longitudinal phase space can be simulated independently of the transverse phase space. Linear approximations of the beam dynamics are insufficient to fully represent the beam evolution. Several nonlinear effects have a leading role in shaping the final longitudinal bunch profile, for example: the non-linearity of the magnetic chicanes, usually referred to with the T_{566} and U_{5666} terms, the curvature due to the RF accelerating fields, the correlated energy spread introduced by short-range wakefields in the accelerating structures, and the non-linearity of the distribution as it comes from the injector. As mentioned in Section 2.2 we plan to use both `LiTrack` and `Track1D` for this purpose. We have tested those codes and the result is shown in Figure 12.

Beam collective effects such as space charge force and coherent synchrotron radiation are not provided in the default version of these programs. By virtue of this, these codes are specifically devoted to the longitudinal beam dynamics of ultra-relativistic particles. The initial charge distribution can be self-generated by both codes, with pre-determined symmetric or asymmetric distributions, or imported as an external ASCII file. In general, the particle distribution is represented by 6 columns, one column per degree of freedom in the 6-D phase space and one row per particle.

The full simulation of the accelerator must then be performed with 6D tracking codes, such as `ELEGANT` and `PLACET` as described in the previous sections of this report.

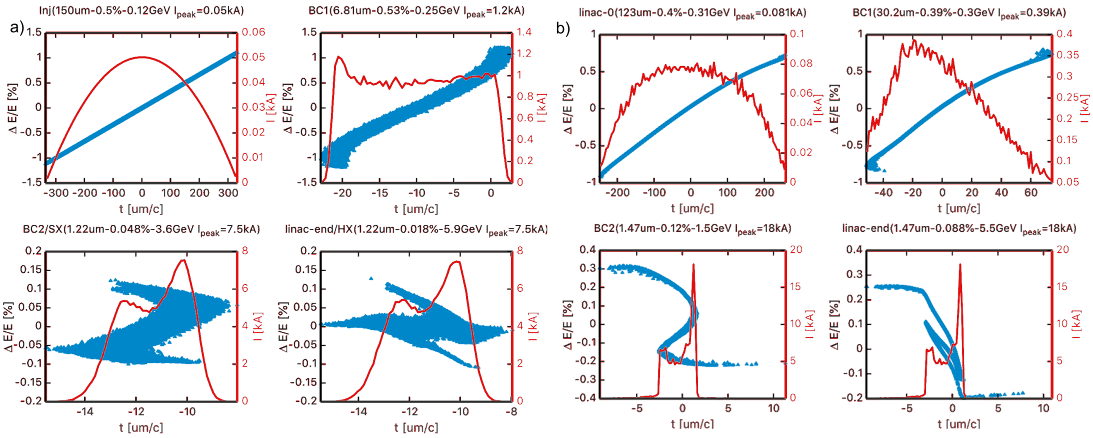

Figure 12: a)Phase space distributions for the S-band injector + X-band lineariser and linacs, as generated by LiTrack. From top left to bottom left, the subplots refer to: after laser heater, exit of BC1, exit of BC2, SX extraction point, HX extraction point. b) Phase space distributions for a full X-band CompactLight, as generated by Track1D. The two chicanes are located at 300 Mev and 1.5 GeV, respectively.

3.2.6 Concluding & remarks

In this section we presented the two codes used for the design of the overall linac and bunch compressors parameters. Both codes implement wakefield effects, which are critical for CompactLight being a wakefield-dominated accelerator. Both tools allow the simulation of the XLS facility from the laser heater up to the linac extraction to the unduluator lines. The interfacing of both codes with high-level numerical languages such as Matlab (LiTrack) or Octave and Python (Track1D), makes the two codes suitable for sophisticated optimisation of the target bunch parameters, as well as for sensitivities studies. Sensitivities studies and multi-parametric optimisation targeting specific bunch attributes, require high computational efficiency. In this respect Track1D seems to offer the best performance in terms of simulation rapidity.

3.3 Comparison of FEL simulation codes and semi-analytical approximations.

Methods for predicting FEL performance comprise a variety of codes, semi-analytic approaches and simulation frameworks. Some of the available codes use approximations for faster and simpler estimations of the FEL performance. Some others provide a deeper insight into the FEL process, compromising on speed. As WP6 will carry out start to end simulations covering the beam transport from the cathode to the end of the undulator, the FEL code to be used should allow an easy integration with the rest of the software framework. This involves implementing (or adapting existing) wrappers and adaptors to allow the interface between different codes.

3.3.1 Brief description of available codes and semi-analytic approximations.

In the following, the Ming-Xie [55] and Dattoli [56] semi-analytic formalisms are described briefly, together with the main codes which are extensively used by the partners of the collaboration: PERSEO[33] and GENESIS[11, 57]. The characteristics of each code are presented and a small hard X-ray study case is carried out to compare the output predictions.

3.3.1.1 Semi-analytic formalisms proposed in order to quantify the FEL performance

Ming-Xie semi-analytic formalism The 1D theory provides a characterisation of the FEL performance via the FEL or Pierce parameter [58, 59],

$$\rho = \frac{1}{2\gamma}\left(\frac{I_0}{I_A}\right)^{\frac{1}{3}}\left(\frac{\lambda_u K f_B}{2\pi\sigma_x}\right)^{\frac{2}{3}} \tag{4}$$

Here $\gamma = E_e/m_e$, E_e is the beam energy, m_e is the electron mass at rest, σ_x is the rms transverse radius of the electron beam, I_0 is the peak current, K is the undulator parameter, λ_u is the undulator period, $I_A = 4\pi\varepsilon_0 m_e c^3/e$ the Alfvén current and ε_0 is the vacuum permittivity constant. The factor f_B relates to the coupling between the electrons and the radiation field and depends on the undulator type

$$f_B = \begin{cases} J_0\left(\frac{K^2}{4+2K^2}\right) - J_1\left(\frac{K^2}{4+2K^2}\right) & \text{for a planar undulator} \\ 1 & \text{for a helical undulator} \end{cases} \tag{5}$$

The gain length can be expressed in terms of the Pierce parameter as follows [30]

$$L_{g,1D} = \frac{\lambda_u}{4\sqrt{3}\pi\rho} \tag{6}$$

The physical description provided by the 1D FEL theory does not take into account the impact of the finite beam emittance ε, diffraction or the role of the energy spread (σ_γ/γ) in the FEL dynamics. Ming-Xie [55] produced a parameterization which redefined the 1D gain length accounting for the effects not considered in the 1D theory. The fitting model assumes a constant electron beam current. The gain length is recalculated in terms of a correction factor Λ as follows

$$L_g = L_{g,1D}\left[1+\Lambda\right] \tag{7}$$

Λ depends on four scaled parameters and is defined as [30];

$$\begin{aligned}\Lambda(\eta_d, \eta_\varepsilon, \eta_\sigma) = a_1\eta_d^{a_2} + a_5\eta_\gamma^{a_6} + a_7\eta_\varepsilon^{a_8}\eta_\gamma^{a_9} \\ + a_{10}\eta_d^{a_{11}}\eta_\gamma^{a_{12}} + a_{13}\eta_d^{a_{14}}\eta_\varepsilon^{a_{15}} + a_{16}\eta_d^{a_{17}}\eta_\varepsilon^{a_{18}}\eta_\gamma^{a_{19}}\end{aligned} \tag{8}$$

The scaled parameters accounts for the reduction of gain from the 1-D condition due to several effects;

- Gain reduction due to diffraction, $\eta_d = \lambda/(4\pi\sigma_x^2)L_{g,1D}$.
- Gain reduction due to finite emittance, $\eta_\varepsilon = (4\pi\varepsilon/\lambda)(L_{g,1D}/\beta)$.
- Gain reduction to energy spread, $\eta_\gamma = (\sigma_\gamma/\gamma)(L_{g,1D}/\lambda_u)$
- The additional fourth parameter, the frequency detuning, is optimised in such a way that the gain length is at its shortest.

Table 10: Set of fitting coefficients for the Ming-Xie parameterization.

$a_1 = 0.45$	$a_2 = 0.57$	$a_3 = 0.55$	$a_4 = 1.6$	$a_5 = 3$	$a_6 = 2$	$a_7 = 0.35$
$a_8 = 2.9$	$a_9 = 2.4$	$a_{10} = 51$	$a_{11} = 0.95$	$a_{12} = 3$	$a_{13} = 5.4$	$a_{14} = 0.7$
$a_{15} = 1.9$	$a_{16} = 1140$	$a_{17} = 2.2$	$a_{18} = 2.9$	$a_{19} = 3.2$		

The set of 19 coefficients ($a_i, i = 1, 2, \cdots, 19$) given in Eq. 8 have been checked against 3-D simulation codes and found by fitting as in Table 10 [30, 59].

Finally the saturation power and saturation length are calculated from the 3D gain length in Eq. (7) using the correction factor given by [55],

$$P_{\text{sat}} = \frac{1.6}{\left(1+\Lambda\right)^2} \rho P_{\text{beam}} \tag{9}$$

$$L_{\text{sat}} = L_g \ln\left(\frac{P_{\text{sat}}}{\alpha P_0}\right) \tag{10}$$

where $P_{\text{beam}} = E_{\text{beam}} I_0/e$, α =1/9 and P_0 is the initial radiation power.

Saldin et al. developed an analytic formalism to describe the coherence properties of a SASE FEL [60]. The coherence time at saturation is defined in terms of the number of cooperating electrons $N_c = I_0\lambda/2\pi ce\bar{\rho}$ as

$$\tau \approx \frac{\lambda}{2\pi c\bar{\rho}} \sqrt{\frac{\pi \ln\left(N_c\right)}{18}} \tag{11}$$

with $\bar{\rho} = \rho D^{\frac{1}{3}}$, the scaled Pierce parameter. The parameter D is the diffraction parameter given by D=$4\pi\Gamma\sigma_x^2/\lambda$. The gain parameter Γ in the diffraction parameter is shown to be

$$\Gamma = \sqrt{\frac{8\pi^2 I_0 K^2 f_B^2}{I_A \lambda \lambda_u \gamma^3}} \tag{12}$$

Saldin et al. found a fitting formula to find the degree of transverse coherence at saturation[59, 60]

$$\zeta_{\text{sat}} = \frac{1.1\hat{\varepsilon}^{\frac{1}{4}}}{1+0.15\hat{\varepsilon}^{\frac{9}{4}}}, \qquad \text{with } \hat{\varepsilon} = 2\pi\varepsilon/\lambda\text{, the scaled emittance} \tag{13}$$

The degeneracy parameter δ (associated with the number of photons per coherent state) is found to be proportional to the coherence time, Eq. (11) and the degree of transversal coherence, Eq. (13)

$$\delta = \dot{N_{\text{ph}}} \tau_c \zeta \tag{14}$$

where $\dot{N_{\text{ph}}}$ is the photon flux. The peak brilliance (corresponding to the transversely coherent spectral flux) is defined in terms of the degeneracy parameter and the resonant wavelength,

$$B_r = \frac{4\sqrt{2}c\delta}{\lambda^3}. \tag{15}$$

Further calculations of the degeneracy parameter allows the peak brilliance to be expressed in terms of the peak current I_0, the beam energy E_e and the radiation wavelength as: [59, 60]

$$B_r \approx 4.5 \times 10^{31} \times \frac{I[kA]E_e[GeV]}{\lambda[\AA]}\hat{\delta} \quad [\text{photons s}^{-1}\ \text{mm}^{-2}\text{mrad}^{-2}(0.1\%\ \text{bandwidth})^{-1}]. \tag{16}$$

Here $\hat{\delta}$ is the scaled degeneracy parameter expressed in terms of $\hat{\eta} = P_{\text{radiation}}/(\bar{\rho}P_{\text{beam}})$ and the scaled coherence time $\hat{\tau}_c = 2\pi c\bar{\rho}\tau_c/\lambda$ as

$$\hat{\delta} = \hat{\tau}_c\hat{\eta}\zeta \tag{17}$$

The semi-analytic parametrization by Ming-Xie, together with the analytic description of temporal coherence by Saldin et al., give an estimate of some of the figures of merit to characterise the FEL output.

Semi-analytic formalism by Dattoli [56]: From the Pierce ρ parameter defined in Eq.(4), a set of simple and accurate scaling formulae has been derived [56, 61–63]. A Mathematica$^{\text{TM}}$ platform [64] is available to run the associated semi-analytic code and allows a fast preliminary design of FEL sources.

In particular, this set of formulae is able to provide the exact analytic form of the FEL peak power growth as a function of the longitudinal propagation coordinate z:

$$\begin{aligned} P(z) &= P_0\frac{A(z)}{1+\frac{P_0}{P_S}[A(z)-1]} \qquad (18)\\ A(z) &= \frac{1}{9}\left[3+2\cosh\left(\frac{z}{L_{g,1D}}\right)+4\cos\left(\frac{\sqrt{3}z}{2L_{g,1D}}\right)\cosh\left(\frac{z}{2L_{g,1D}}\right)\right] \end{aligned}$$

depending upon the gain length defined in eq.(6).

The effect of inhomogeneous broadening, namely the gain reduction due to non-ideal electron beam qualities (significant energy spread and normalized emittance) can be easily embedded in the previous formulae. The use of the μ parameters, expressed in terms of the normalized emittance, RMS energy spread and Pierce parameter allows a fairly straightforward estimate of these effects, which contributes to increase the gain length. In fact, due to the energy spread we have the following correction function χ:

$$L_g = \chi\left(\rho, \frac{\sigma_\gamma}{\gamma}\right)L_{g,1D} \simeq \left(1+\frac{0.185\sqrt{3}}{2}\mu_\varepsilon^2\right)L_{g,1D}, \quad \mu_\varepsilon = 2\frac{\sigma_\gamma/\gamma}{\rho} \tag{19}$$

where χ is the expansion result of the μ_ε ratio. The effective saturation power decreases accordingly, depending on the same χ functionof the energy spread:

$$\Phi(\chi) = e^{-\chi(\chi-1)} + \sqrt{2}\frac{\chi-1}{\chi^3} \tag{20}$$

Then, in a way similar to eq.(9), we have the following corrected quantities, at saturation:

$$P_{\text{sat}} = \sqrt{2}\Phi(\chi)\rho P_{\text{beam}} \tag{21}$$

$$L_{\text{sat}} = 1.066 L_g \ln\left(\frac{9P_{\text{sat}}}{P_0}\right) \tag{22}$$

The reliable estimate of the latter two quantities demands also for considering inhomogeneous broadening effects due to three dimensional diffraction contributions, which modify the Pierce parameter by introducing the μ_D diffraction parameter, as described below:

$$\mu_D = \frac{\lambda\lambda_u}{(4\pi\sigma_T)^2\rho},\ \rho_D = \mathscr{F}(\mu_D)\rho,\ \mathscr{F}(\mu_D) = \frac{1}{\sqrt[3]{1+\mu_D}} \tag{23}$$

where we considered a transversely symmetric electron beam with $\sigma_x = \sigma_y = \sigma_T$, and normalized emittances $\varepsilon_x = \varepsilon_y$. As a consequence, putting both sources of gain reduction together, we finally have:

$$P_{\text{sat,3D}} = \sqrt{2}\Phi(\chi)\left(\frac{L_{g,1D}}{L_g}\right)^2 \rho_D P_{\text{beam}}, \tag{24}$$

$$L_{\text{sat,3D}} = 1.066 L_g\left(\rho_D, \frac{\sigma_\gamma}{\gamma}\right) \ln\left(\frac{9P_{\text{sat}}}{P_0}\right) \tag{25}$$

3.3.1.2 Time dependent Simulations

The theoretical approaches summarized in the previous sections allow one to obtain analytic estimates of some of the features of the FEL. These analytic formulations are useful in narrowing the range of the input parameters for the simulation, but specific effects such as magnetic errors or alignment errors, or the effects of specific distributions, are not considered. For this reason simulation codes are widely used in the design of FEL sources and the validation of simulation results against available experimental data and cross comparison of their results is important. We propose to use two benchmarked codes in the design of CompactLight and in this section we summarize their specifications.

Perseo: `PERSEO` is a library of functions developed for the one dimensional simulation of FEL dynamics within the Mathcad® framework [10, 33]. The core of the library consists of the routines solving the pendulum-like FEL equations coupled with the field equations that govern the FEL longitudinal dynamics, and including self-consistently the field variables for the higher order harmonics.

The radiation field in `PERSEO` is the superposition of slowly varying complex amplitudes

$$a_n = |a_n|e^{i\varphi_n}, \quad E(z,t) = \sum_n \tilde{E}_n a_n e^{i(k_n z - \omega_n)} \tag{26}$$

for each harmonic n. The evolution of these amplitudes is described by the following equations:

$$\frac{\partial \Re e\,[a_n(\tau_u)]}{\partial \tau_u} = -2\pi g_n \langle \cos(n\theta_\ell(\tau_u))\rangle,$$
$$\frac{\partial \Im m\,[a_n(\tau_u)]}{\partial \tau_u} = 2\pi g_n \langle \sin(n\theta_\ell(\tau_u))\rangle \tag{27}$$

where $\tau_u = \beta_z ct/L_u$ is the dimensionless interaction time, scaled by the undulator length, $L_u = N\lambda_u$, and $\beta_z c$ is the electron beam velocity. The coupling coefficient per each harmonic is given by:

$$g_n = 2\pi\left(\frac{N}{\gamma}\right)^3 [\lambda_u K f_B(n,K)]^2 \frac{j_{peak}}{I_A} \tag{28}$$

The phase of the ℓ-th electron depends on the associated undulator wave-vector, the radiation wave-vector and frequency:

$$\theta_\ell = (k - k_u)z_\ell - \omega t \tag{29}$$

The ℓ-th electron motion is described by the pendulum-like equations:

$$\begin{aligned} \frac{d\theta_\ell}{d\tau_u} &= v_\ell, \\ \frac{dv_\ell}{d\tau_u} &= \sum_n \cos(n\theta_\ell)\Re e(a_n) - \sin(n\theta_\ell)\Im m(a_n) \end{aligned} \tag{30}$$

where $v_\ell = 2\pi N(\omega_\ell - \omega)/\omega$ describes the frequency shift of the ℓ-th particle resonance from the reference frequency.

Phase space quantities generation and manipulation within a number of different devices are made possible through a series of Mathcad® worksheets.

In an FEL oscillator or seeded facility, when the transverse properties of the radiation may be considered as a constraint of the problem, the coupling coefficient of Eq.(28) has to be corrected by a proper filling factor. When the radiation size is the result of the balance between diffraction and focusing induced by the gain, as in a single-pass FEL, a filling factor coefficient may be derived from the Ming-Xie scaling laws by calculating the ratio between the Ming-Xie factor with and without diffraction effects [55, 56].

Genesis: `GENESIS`, as described in Section 2.3, is a time-dependent, 3D code [11, 57]. `GENESIS` is characterised by the distribution of the discretized radiation field and the electron macro-particles on a Cartesian mesh. The code applies the Slowly Varying Envelope Approximation (SVEA) to the field which is described by a fast-oscillating term and an envelope which slowly varies in phase and amplitude. Further approximations involve a paraxial current, such that the wave equation is reduced to its paraxial form, and Wigner averaging. The field is integrated via the Alternating Direction Implicit method. The electron longitudinal parameters are integrated using a 4^{th} order Runge Kutta algorithm [65]. Since the dynamics of electrons and the radiation field are evaluated at the same position of the Cartesian grid, the leapfrog method is used to avoid numerical inaccuracies. The loading of the macro-particles is done via Hammersley sequences [57, 66]. Later updates of `GENESIS` allow the simulation of each individual electron rather than representative macro-particles (which reduces the factor of error in the noise statistics)[67].

Existing software frameworks (such as the simulation toolkit OCELOT implemented by the European XFEL Project [68]) contain routines and functions in Python which allow the analysis of the post-processing of data. Therefore, integration of `GENESIS` into a start-to-end simulation environment can be done. The flexibility of `GENESIS` has allowed it to be used to simulate many different schemes including self-seeding [69], High Gain Harmonic Generation (HGHG) [70] and generation of a few cycle pulses via a mode locking afterburner [**Dunning2013**].

3.3.2 Study case: Assessment of a hard X-Ray FEL

A study case is carried out to determine the performance of a cryogenic permanent magnet undulator (CPMU) based FEL to benchmark the FEL codes and semi-analytic approximations.

Table 11: Electron beam parameters.

Electron beam parameter	**Value**
Beam Energy	5.5 GeV
Peak Current	5 kA
Shape of Current distribution	Flat-top
Bunch length	1.64 μm
Bunch Charge	27 pC
Normalised $\varepsilon_{\text{x,y}}$	0.2 mm-mrad
RMS slice energy spread	0.01$\%$

Table 12: Undulator parameters for the CPMU.

Undulator parameter	**Value**
Undulator type	Planar
Undulator period	12.87 mm
RMS Undulator parameter	0.628
Undulator module length	2 m

The electron beam has the parameters listed in Table 11. The CPMU is tuned to a resonant wavelength of 0.0756 nm, corresponding to a photon energy of 16 keV and has the parameters listed in Table 12. The optimised average β function of 9m minimised the gain length. The beam current has a flat-top distribution.

Estimations of FEL performance were made using the Xie and Dattoli models with results shown on Table 13). The gain length and saturation length agreed well, to within a relative difference $\Delta L_{\text{sat}}/L_{\text{Xie-sat}}$ of approximately 6%. However, the Dattoli model predicts a 22.53$\%$ increase in saturation power compared to Ming Xie.

Table 13: Estimations of FEL performance from the semi-analytic models.

Figure of merit	**Ming-Xie**	**Dattoli**
P_{sat} [GW]	17.97	22.02
L_{sat} [m]	20.81	19.47
L_{gain} [m]	1.12	0.974

The FEL figures of merit obtained from the time-dependent simulations using both codes (GENESIS and PERSEO) are summarised in Table 14. It should be noted that for the parameters used the bunch length is much longer than the total slippage length so that the saturation length and peak power derived from the time-dependent simulations can be directly compared to those found from the semi-analytic models. Ten different noise realisations were run in the case of GENESIS to account for SASE shot-to-shot fluctuations. The results in Table 14 (displayed in Figures 15 as the thicker lines) correspond to the average over all noise realisations. The pulse energy curves for both codes are shown in Figure 13. The zoomed region shows the difference in the linear regime between PERSEO and GENESIS . The calculated spectrum (shown in Figure 14) is shown to be different, but the main spectral contribution to SASE comes from the same wavelength. The dark red line in the GENESIS results is the

Table 14: Estimations of FEL figures of merit at saturation, and running time of the simulation for the CPMU. The peak brilliance (B_{sat}) is measured in units of ph/s/mm^2/mrad^2/0.1%bw. The GENESIS results are averaged over ten noise realisations.

Figure of merit	PERSEO	GENESIS
P_{sat}[GW]	11.4	5.69
L_{sat}[m]	21.62	21.69
E_{pulse}[μJ]	60	31.09
$N_{photons}$	2.3×10^{10}	1.28×10^{10}
Bandwidth[%]	0.055	0.064
B_{sat}	4.2×10^{32}	1.41×10^{32}
Running time	$<$ 5 min	90 min (25 processors)

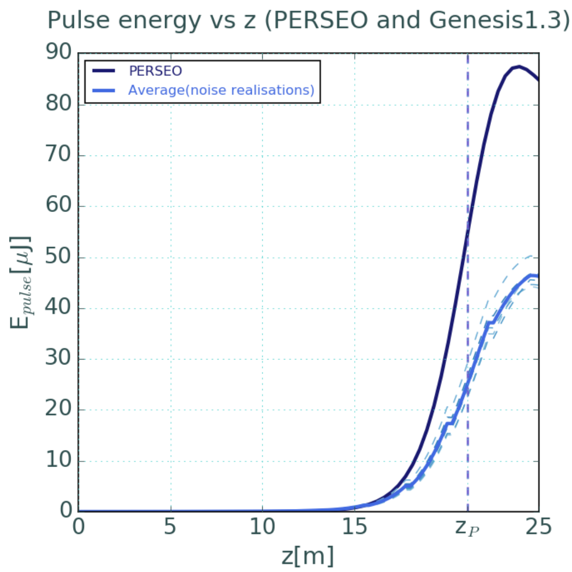

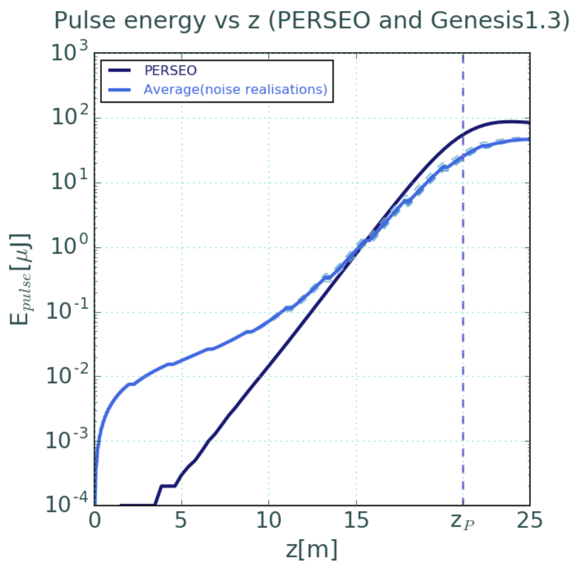

Figure 13: Pulse energy as calculated by GENESIS and PERSEO(left: linear scale and right: logarithmic scale). The thicker brighter blue line is the average over all noise realisations from the Genesis simulations. The lighter dotted blue lines are the energy curves per noise realisation.

average over noise realisations.

The comparison between the two codes shows that the saturation lengths appear consistent, but the average peak power, pulse energy and photon flux at saturation obtained from GENESIS are around 50 % of those obtained via PERSEO . The peak brilliance at saturation obtained via PERSEO is almost three times that from GENESIS . The difference may be explained by the fact that PERSEO only supports the fundamental transverse mode whereas GENESIS supports a larger number of transverse high order modes in the Cartesian grid calculation, which contribute less to the total radiation in the linear regime and at saturation[71].

A further comparison of the peak brilliance is done using the semi-analytic model (Eq. (15)) which gives a brilliance of 1.11×10^{32} ph/s/mm^2/mrad^2/0.1%bw. This value is 78 % and 26%

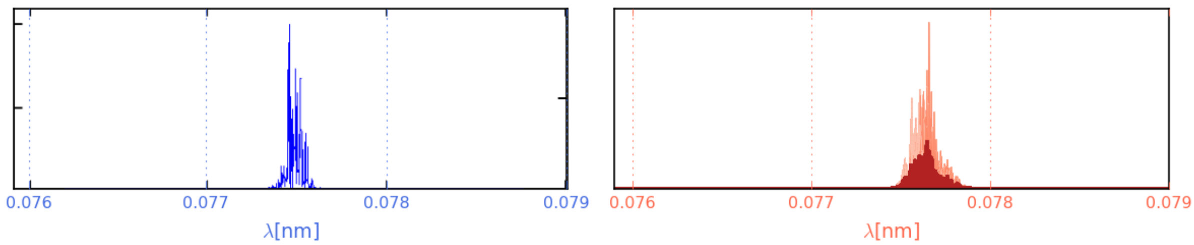

Figure 14: Spectrum as calculated by and PERSEO (left) and GENESIS (right)

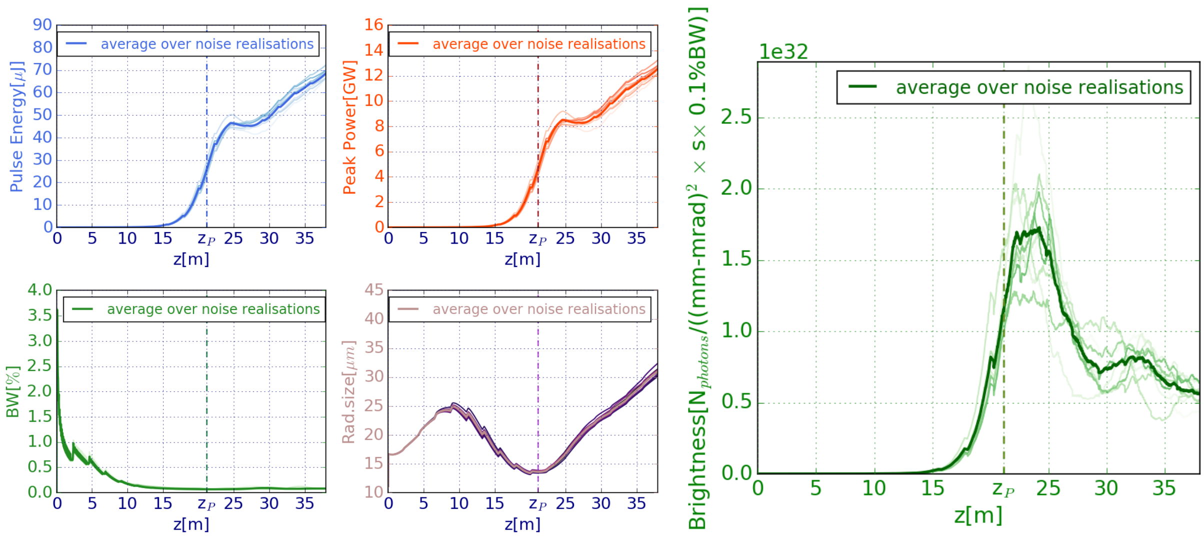

(a) (b)

Figure 15: GENESIS simulation for CMU undulator. (a) shows the evolution of the pulse energy, average of peak power over all electron beam slices, bandwidth and radiation size. (b) shows the peak brilliance of the coherent radiation along the undulator.

of the value obtained for the GENESIS and PERSEO simulations respectively.

An important aspect is the time it takes to run the simulations. As seen in Table 14, PERSEO was fast compared to GENESIS as would be expected when comparing a 1D code with a full 3D code. However, the running time in GENESIS can be optimised via a modification of the input parameters. In order to quantify an example of this, several simulations were performed with a shorter bunch length (0.18 μm) and a different number of macro-particles per slice, n. The results are displayed in Figure 16. The pulse energy at saturation converges for $n > 1000$ indicating that n can safely be reduced to this number to speed up the simulation without effecting the result. Other parameters can also be optimised, for example the dimension and resolution of the Cartesian Grid.

For S2E simulations the ability to interface the FEL code with beam dynamics and optical propagation codes is important. PERSEO is a 1D simulation code so cannot be directly interfaced with 3D lattice codes such as ELEGANT , ASTRA and GPT. However, it is a natural candidate to be interfaced with a 1D beam dynamics code such as LiTrack . In that regard, GENESIS is the better option if a full 3D S2E environment is envisioned because interfaces between ASTRA and GENESIS and ELEGANT and GENESIS have been implemented in

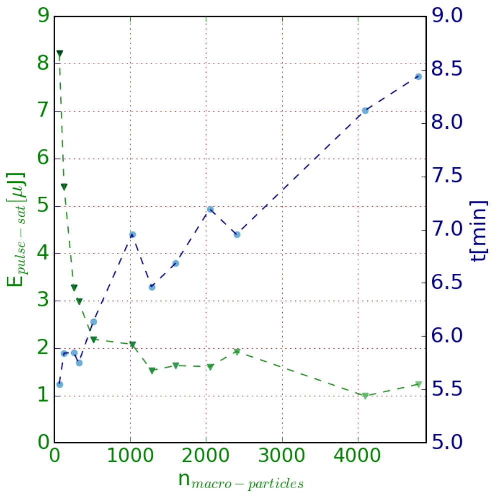

Figure 16: Pulse energy at saturation and time duration per simulation as a function of macro-particles number n for GENESIS.

the OCELOT[68] and SDDS-Toolkit[28], respectively, as has an interface to OPC, an optical propagation code [72]. A LiTrack and PERSEO setup can therefore be used for initial, quick estimations those scenarios where the longitudinal dynamics are the main subject of concern. For more detailed simulations, GENESIS provides a more comprehensive solution.

3.3.3 Concluding remarks

An introduction to the simulation codes and semi-analytic models used by the partners of the collaboration has been given, including a study case to compare output. Bench-marking between GENESIS and PERSEO has previously been carried out by Giannessi et al. [33, 73] to simulate the dynamics of higher order harmonics and the performance of the SPARC facility [71], showing agreement in some of the figures of merit of the FEL performance (linear regime, gain of harmonic components amongst others). The study case reported here, in agreement with [71], shows that PERSEO predicts a higher peak power, pulse energy and brilliance then GENESIS. The time duration can be an issue to consider as PERSEO is quicker. However, for those scenarios in which 3D effects are more prominent and cannot be neglected GENESIS provides a more natural choice. The time it takes for GENESIS to run a simulation can be optimised via the Cartesian grid properties or the macro-particle number after appropriate convergence tests. In terms of interfacing GENESIS and PERSEO with other beam dynamics simulation codes the dimensionality of the codes is relevant—-GENESIS is fully 3D whereas PERSEO is 1D with corrections applied to account for 3D effects. PERSEO can be interfaced to 1D beam dynamics simulation codes for faster design studies. If a more comprehensive study is required (including 3D effects), GENESIS is the right fit, as it can be interfaced to 3D beam dynamics and optical propagation codes.

4 Conclusion

There are several sources of non linear collective effects that may play an important role in the design of short wavelength free electron lasers. We have analyzed the three regimes with this report

- Injection
- Acceleration and compression
- FEL process

We have used various investigation tools devoted to the simulation of the specific regimes and offered the opportunity to analyze. Since the the simulation of charged particles interacting with electromagnetic field has too wide conditions which has to be considered, the S2E simulation cannot be accomplished by a single code. This report covers the summary of some of the simulation tools to analyze beam generation, bunch compression, collective effects in linacs and the FEL process. Some of these tools are going to be integrated in order to perform S2E implementation.

In general, to start S2E design of a facility like ComplactLight, we may first use analytic approximations by including the most of the physical aspects of the specific problem to avoid complexity of the implementation and to gain time in calculation. In the second step we use the numerical implementation which includes some "smart" theoretical approach in accordance with some physical approximations. This step shall allow addressing some specific issue relevant to the problem with a fast relaxation of the usually large number of parameters involved. At the final stage we implement combined collective physical aspects into one simulation to seek a methodology that preserves as much information as possible between the regimes mentioned above. At these stage, we generally use large number of marcroparticles in 6D phase spaces in order to have better statistical result.

The choice of simulation tools depends several crucial criteria; simulation time, the amount of data when 6D phase spaces are used, the output format etc... For example the interface refers not only to the human interface for the analysis and visualization of the results but also the code-to-code interfaces necessary to perform a self consistent S2E simulation of the whole facility using multiple codes. The necessity of different codes for handling different regime requires change of phase spaces in a compatible format between different programs. We plant to develop a translator for multiple programs. We need to agree a common well known exchange format between codes, for example SDDS or HDF5. The last, but not least, aspect is the documentation and availability of the source codes. The open source nature of a code is important for the user who does not want to be faced with a 'black box' but wants the opportunity to directly analyze the source code and the underlying equations and algorithms she or he is dealing with.

To provide the key parameters and performance estimates of CompactLight facility we need to develop consistent tool for modelling the machine. In addition to the collective effects we need to implement static errors, error correction, and pulse-to-pulse jitter etc... into the tool. The tool shall provide highly automated and flexible modeling, thus permitting routine execution of hundreds of simulations for tolerance, correction, and jitter studies.

References

[1] G. D'Auria et al., *The CompactLight Design Study Project*, Proceedings of International Particle Accelerator Conference 2019, JACoW, 2019, TUPRB032, DOI: 10.18429/JACoW-IPAC2019-TUPRB032.

[2] K. Flöttmann, *Astra: A space charge tracking algorithm*, 2011.

[3] M. De Loos, S. Van der Geer, *General Particle Tracer: A 3D Code for Accelerator and Beam Line Design*, Proc. EPAC96, 1996, p. 1241, URL: https://accelconf.web.cern.ch/AccelConf/e98/PAPERS/THP18F.PDF.

[4] L. M. Young, J. Billen, *The particle tracking code PARMELA*, PAC03, 2003.

[5] A. Latina, *RF-Track: beam tracking in field maps including space-charge effects - features and benchmarks*, LINAC 2016: the 28th international Linear Accelerator conference, 2017, DOI: 10.18429/JACoW-LINAC2016-MOPRC016.

[6] M. Borland, *ELEGANT: A flexible SDDS-compliant code for accelerator simulation*, tech. rep., 2000, DOI: 10.2172/761286.

[7] A. Latina et al., *Recent Improvements in the Tracking Code Placet*, Epac (2008).

[8] K. L. F. Bane, P. Emma, *LiTrack: A fast longitudinal phase space tracking code with graphical user interface*, Proceedings of the IEEE Particle Accelerator Conference, 2005, ISBN: 0780388593, DOI: 10.1109/PAC.2005.1591786.

[9] A. Latina, *Track1D*, Geneva, Switzerland, URL: https://gitlab.cern.ch/XLS-Git/WP6/tree/master/simulation_codes/beam_dynamics/Track1D.

[10] L. Giannessi, *PERSEO FEL-CAD Library*, 2007, URL: http://www.perseo.enea.it/.

[11] S. Reiche, *GENESIS 1.3 User Manual*, tech. rep., URL: http://genesis.web.psi.ch/download/documentation/genesis_manual.pdf.

[12] S. Reiche, *GENESIS 1.3: a fully 3D time-dependent FEL simulation code*, Nuclear Instruments and Methods in Physics Research Section A: Accelerators, Spectrometers, Detectors and Associated Equipment **429** (1999) 243, ISSN: 0168-9002, DOI: 10.1016/S0168-9002(99)00114-X, URL: https://www.sciencedirect.com/science/article/pii/S016890029900114X?via%3Dihub.

[13] R. Ruth, *An Overview of Collective Effects in Circular and Linear Accelerators*, tech. rep., SLAC Publication: SLAC-PUB-4948, 1989.

[14] B. E. Carlsten, *Space Charge Induced Emittance Compensation in High Brightness Photoinjectors*, Part. Accel. **49** (1995) 27, URL: http://cds.cern.ch/record/1108320.

[15] M. Pedrozzi, *SwissFEL Injector Conceptual Design Report*, tech. rep., PSI, 2010.

[16] J. L. e. a. Warren, *Reference manual for the POISSON/SUPERFISH Group of Codes*, tech. rep. LA-UR-87-126, 1987, DOI: 10.2172/10140827.

[17] *{ANSYS} Electronics Desktop website*, \url{http://www.ansys.com/products/electronics/ansys-electronics-desktop}.

[18] C. Limborg et al., *Code comparison for simulations of photo-injectors CODE COMPARISON FOR SIMULATIONS OF PHOTO-INJECTORS* (2003), DOI: 10.2172/833072.

[19] I. Ben-zvi, I. V. Bazarov, *Summary , Working Group 1 : Electron guns and injector designs*, **557** (2006) 337, DOI: 10.1016/j.nima.2005.10.097.

[20] N. R. Neveu et al., *BENCHMARK OF RF PHOTOINJECTOR AND DIPOLE USING ASTRA , GPT , AND OPAL* () 1194.

[21] I. V. Bazarov et al., *Benchmarking of 3D space charge codes using direct phase space measurements from photoemission high voltage dc gun*, **100703** (2008) 1, DOI: 10.1103/PhysRevSTAB.11.100703.

[22] C. Ronsivalle et al., *SIMULATIONS OF THE EMITTANCE COMPENSATION IN PHOTOINJECTORS AND COMPARISON WITH SPARC MEASUREMENTS SHORT REVIEW OF EMITTANCE* () 21.

[23] E. L. Saldin, E. A. Schneidmiller, M. V. Yurkov, *On the coherent radiation of an electron bunch moving in an arc of a circle*, Nuclear Instruments and Methods in Physics Research, Section A: Accelerators, Spectrometers, Detectors and Associated Equipment (1997), ISSN: 01689002, DOI: 10.1016/S0168-9002(97)00822-X.

[24] S. Heifets, G. Stupakov, S. Krinsky, *Coherent synchrotron radiation instability in a bunch compressor*, Phys. Rev. ST Accel. Beams **5** (2002) 64401, DOI: 10.1103/PhysRevSTAB.5.064401, URL: https://link.aps.org/doi/10.1103/PhysRevSTAB.5.064401.

[25] Stanford Linear Accelerator Center, *Linac Coherent Light Source (LCLS) Conceptual Design Report*, Slac-R-593 (2002), DOI: 10.2172/1029479.

[26] J. W. Eaton et al., *GNU Octave version 5.1.0 manual: a high-level interactive language for numerical computations*, 2019.

[27] L. Deniau et al., *MAD-X Users guide*, tech. rep., CERN, 2019, URL: http://mad.web.cern.ch/mad/.

[28] M. Borland et al., *User's Guide for SDDS Toolkit*, tech. rep., Advance Photon Source, 2007, URL: https://ops.aps.anl.gov/manuals/SDDStoolkit/SDDStoolkit.html.

[29] Z. Huang, K.-J. Kim, *Review of x-ray free-electron laser theory*, Physical Review Special Topics - Accelerators and Beams **10** (2007) 034801, ISSN: 1098-4402, DOI: 10.1103/PhysRevSTAB.10.034801, URL: https://link.aps.org/doi/10.1103/PhysRevSTAB.10.034801.

[30] D. E. Kim et al., *Undulator commissioning experience at PAL-XFEL*, Proceedings of IPAC2017, JACoW, Copenhagen, Denmark, 2017, TUPAB087, ISBN: 9783954501823.

[31] H.-D. Nuhn, *Overview of SASE free-electron laser simulation codes*, vol. 3614, 1999, DOI: 10.1117/12.352658, URL: https://doi.org/10.1117/12.352658.

[32] G. Dattoli, S. Pagnutti, P. L. Ottaviani, *PROMETEO: A Fortran77 code for Free Electron Lasers*, URL: http://www.afs.enea.it/software/prometeo/index-test.html.

[33] L. Giannessi, *OVERVIEW OF PERSEO, A SYSTEM FOR SIMULATING FEL DYNAMICS IN MATHCAD*, 2006 Free Electron Laser Conference, 2006.

[34] W. M. Fawley, *A User Manual for GINGER and its Post-Processor XPLOTGIN*, tech. rep., Lawrence Berkeley National Laboratory, 2004.

[35] L. T. Campbell, B. W. J. McNeil, *Puffin: A three dimensional, unaveraged free electron laser simulation code*, Physics of Plasmas **19** (2012) 093119, DOI: 10.1063/1.4752743, URL: http://aip.scitation.org/doi/10.1063/1.4752743.

[36] R. A. Jong, W. M. Fawley, E. T. Scharlemann, *Modeling Of Induction-Linac Based Free-Electron Laser Amplifiers*, Proceedings SPIE, ed. by D. L. Bullock, 1989, p. 18, DOI: 10.1117/12.951306, URL: http://proceedings.spiedigitallibrary.org/proceeding.aspx?doi=10.1117/12.951306.

[37] E. Saldin, E. Schneidmiller, M. Yurkov, *FAST: a three-dimensional time-dependent FEL simulation code*, Nuclear Instruments and Methods in Physics Research Section A: Accelerators, Spectrometers, Detectors and Associated Equipment **429** (1999) 233, ISSN: 0168-9002, DOI: 10.1016/S0168-9002(99)00110-2, URL: https://www.sciencedirect.com/science/article/pii/S0168900299001102.

[38] H. P. Freund et al., *Three-dimensional, time-dependent simulation of free-electron lasers with planar, helical, and elliptical undulators*, New Journal of Physics **19** (2017) 023020, DOI: 10.1088/1367-2630/aa59f1, URL: http://stacks.iop.org/1367-2630/19/i=2/a=023020?key=crossref.108a05f3b6ae699c38640e203fa5845d.

[39] Z. Huang, K.-J. Kim, *Spontaneous and amplified radiation at the initial stage of a SASE FEL*, Nuclear Instruments and Methods in Physics Research Section A: Accelerators, Spectrometers, Detectors and Associated Equipment **507** (2003) 65, ISSN: 0168-9002, DOI: 10.1016/S0168-9002(03)00839-8, URL: https://www.sciencedirect.com/science/article/pii/S0168900203008398.

[40] G. Marcus et al., *FEL code comparison for the production of harmonics via harmonic lasing*, Proceedings of FEL Conference, Basel, Switzerland, 2014, URL: http://www.slac.stanford.edu/cgi-wrap/getdoc/slac-pub-16082.pdf.

[41] B. Garcia et al., *Comparing FEL codes for advanced configurations*, Proceedings of FEL Conference, Santa Fe, NM, USA, 2017, MOP016, ISBN: 9783954501793, DOI: 10.18429/JACoW-FEL2017-MOP016, URL: http://accelconf.web.cern.ch/AccelConf/fel2017/papers/mop016.pdf.

[42] R. Neal, *THE STANFORD TWO-MILE LINEAR ACCELERATOR*, tech. rep. October, 1966, p. 340.

[43] A. Giribono et al., *ELI-NP GBS STATUS* () 880.

[44] D. Alesini et al., *High Power Test Results of the ELI-NP S-Band Gun Fabricated with the New Clamping Technology Without Brazing*, Proceedings of the 8th International Particle Accelerator Conference (IPAC2017) **1** (2017) 3.

[45] A. D. Debus et al., *Traveling-wave Thomson scattering and optical undulators for high-yield EUV and X-ray sources*, Applied Physics B: Lasers and Optics **100** (2010) 61, ISSN: 09462171, DOI: 10.1007/s00340-010-3990-1.

[46] F. Klaus, *Note on the thermal emittance of electrons emitted by Cesium Telluride photocathodes*, TESLA FEL-Report 1997-01 (1997) 40.

[47] D. H. Dowell, J. F. Schmerge, *Quantum efficiency and thermal emittance of metal photocathodes*, Physical Review Special Topics - Accelerators and Beams **12** (2009) 1, ISSN: 10984402, DOI: 10.1103/PhysRevSTAB.12.074201.

[48] R. Pompili et al., *Recent results at SPARC_LAB*, Nuclear Instruments and Methods in Physics Research, Section A: Accelerators, Spectrometers, Detectors and Associated Equipment **909** (2018) 139, ISSN: 01689002, DOI: 10.1016/j.nima.2018.01.071.

[49] G. A. Loew et al., *Computer calculations of traveling-wave periodic structure properties*, IEEE Transactions on Nuclear Science (1979), ISSN: 15581578, DOI: 10.1109/TNS.1979.4330585.

[50] L. Serafini, J. B. Rosenzweig, *Envelope analysis of intense relativistic quasilaminar beams in rf photoinjectors: A theory of emittance compensation*, Physical Review E **55** (1997) 7565, ISSN: 1063-651X, DOI: 10.1103/physreve.55.7565.

[51] B. Aune, R. H. Miller, *New Method for Positron Production At Slac*, 1979 Linear Accelerator Conference, September, 1979, p. 0.

[52] J. C. Smith et al., *Comparison of tracking codes for the international linear collider*, Proceedings of the IEEE Particle Accelerator Conference, 2007, ISBN: 1424409179, DOI: 10.1109/PAC.2007.4440654.

[53] K. Bane, *Short range dipole wakefields in accelerating structures for the NLC*, SLAC-PUB-9663 (2003).

[54] M. Dohlus, T. Limberg, P. Emma, *Bunch Compression for Linac-based FELs*, 2005.

[55] Ming Xie, *Design optimization for an X-ray free electron laser driven by SLAC linac*, Procedures of IEEE Particle Acceleration Conference, Dallas, TX, USA, 1995, p. 183, DOI: 10.1109/pac.1995.504603.

[56] G. Dattoli et al., *Semi-analytical model of self-amplified spontaneous-emission free-electron lasers, including diffraction and pulse-propagation effects*, Journal of Applied Physics **95** (2004) 3206, ISSN: 0021-8979, DOI: 10.1063/1.1645979, URL: http://aip.scitation.org/doi/10.1063/1.1645979.

[57] S. Reiche aus Jork, *Numerical Studies for a Single Pass High Gain Free-Electron Laser*, PhD thesis, University of Hamburg, 1999, URL: http://genesis.web.psi.ch/download/documentation/genesis_thesis.pdf.

[58] R. Bonifacio, C. Pellegrini, L. Narducci, *Collective instabilities and high-gain regime in a free electron laser*, Optics Communications **50** (1984) 373, ISSN: 0030-4018, DOI: 10.1016/0030-4018(84)90105-6, URL: https://www.sciencedirect.com/science/article/pii/0030401884901056?via%3Dihub.

[59] A. Mak et al., *Undulator Considerations in the Baseline Design of the MAX IV Soft X-Ray Laser*, tech. rep., DEPARTMENT OF PHYSICS and ASTRONOMY UPPSALA UNIVERSITY, 2018, URL: http://uu.diva-portal.org.

[60] E. L. Saldin, E. A. Schneidmiller, M. V. Yurkov, *Statistical and coherence properties of radiation from x-ray free-electron lasers*, New Journal of Physics **12** (2010) 035010, ISSN: 1367-2630, DOI: 10.1088/1367-2630/12/3/035010, URL: http://stacks.iop.org/1367-2630/12/i=3/a=035010?key=crossref.1d6a11bf3834ba2332f40daa9164e0a6.

[61] G. Dattoli et al., *Limits on the Single-Pass Higher Harmonics FEL Operation*, IEEE Journal of Quantum Electronics (1984), ISSN: 15581713, DOI: 10.1109/JQE.1984.1072516.

[62] G. Dattoli et al., *Inhomogeneous broadening effects in high-gain free electron laser operation: A simple parametrization*, Il Nuovo Cimento D (1989), ISSN: 03926737, DOI: 10.1007/BF02450989.

[63] G. Dattoli, P. L. Ottaviani, S. Pagnutti, *Booklet for FEL Design*, ENEA – Edizioni Scientifiche, Frascati, 2007, URL: http://www.fel.enea.it/booklet/pdf/Booklet_for_FEL_design.pdf.

[64] M. Artioli, G. Dattoli, S. Pagnutti, *PARSIFEL: an FEL design and computational tool*, URL: http://www.fel.enea.it/parsifel.html.

[65] v. Frau Dipl-Ing Kathrin Goldammer et al., *Studies of Harmonic Generation in Free Electron Lasers*, PhD thesis, Humboldt University Berlin, 2007, URL: https://edoc.hu-berlin.de/bitstream/handle/18452/16373/goldammer.pdf?sequence=1.

[66] W. Reiher, *Hammersley, J. M., D. C. Handscomb: Monte Carlo Methods. Methuen & Co., London, and John Wiley & Sons, New York, 1964. VII + 178 S., Preis: 25 s*, Biometrische Zeitschrift (2007), ISSN: 00063452, DOI: 10.1002/bimj.19660080314.

[67] S. Reiche, *Update on the FEL code Genesis1.3*, Proceedings of FEL Conference, Basel, Switzerland, 2014, TUP019, ISBN: 9783954501335, URL: http://accelconf.web.cern.ch/AccelConf/FEL2014/papers/tup019.pdf.

[68] I. Agapov et al., *OCELOT: A software framework for synchrotron light source and FEL studies*, Nuclear Instruments and Methods in Physics Research, Section A: Accelerators, Spectrometers, Detectors and Associated Equipment **768** (2014) 151, ISSN: 01689002, DOI: 10.1016/j.nima.2014.09.057, URL: https://www.sciencedirect.com/science/article/pii/S0168900214010882?via%3Dihub.

[69] S. Serkez et al., *Soft x-ray self-seeding simulation methods and their application for the linac coherent light source*, Physical Review Special Topics - Accelerators and Beams (2015), ISSN: 10984402, DOI: 10.1103/PhysRevSTAB.18.030708.

[70] N. R. Thompson, B. W. J. McNeil, *Mode locking in a free-electron laser amplifier*, Physical Review Letters (2008), ISSN: 00319007, DOI: 10.1103/PhysRevLett.100.203901.

[71] L. Giannessi et al., *Self-amplified spontaneous emission for a single pass free-electron laser*, Physical Review Special Topics - Accelerators and Beams **14** (2011) 060712, ISSN: 10984402, DOI: 10.1103/PhysRevSTAB.14.060712, URL: https://link.aps.org/doi/10.1103/PhysRevSTAB.14.060712.

[72] J. G. Karssenberg et al., *FEL-OSCILLATOR SIMULATIONS WITH GENESIS 1.3*, Proceedings of FEL Conference, Berlin, Germany, 2006, URL: https://pdfs.semanticscholar.org/94f6/eef698b4e83a5fd862dcdf6813aab4523b09.pdf.

[73] L. Giannessi et al., *Higher-order harmonics coupling in different free-electron laser codes*, Nuclear Instruments and Methods in Physics Research, Section A: Accelerators, Spectrometers, Detectors and Associated Equipment **593** (2008) 143, ISSN: 01689002, DOI: 10.1016/j.nima.2008.04.075, URL: https://www.sciencedirect.com/science/article/pii/S0168900208006426.